AIAA JOURNAL
Vol. 48, No. 6, June 2010

Integrated Local Petrov–Galerkin Sinc Method for Structural Mechanics Problems

Wesley C. H. Slemp,* Rakesh K. Kapania,† and Sameer B. Mulani‡
Virginia Polytechnic Institute and State University, Blacksburg, Virginia 24060

DOI: 10.2514/1.45892

A novel method for solving static boundary-value problems named the integrated local Petrov–Galerkin sinc method is introduced. The method uses the process of numerical indefinite integration based on the double-exponential transformation to develop basis functions for a local Petrov–Galerkin type numerical method. Because the developed basis functions do not satisfy the Kronecker delta property, essential boundary conditions are imposed using the traditional penalty method and the Lagrange multiplier method. Three basis functions are introduced, and the accuracy and efficiency of the method is examined for two problems: a one-dimensional tapered bar with vanishing tip area and a two-dimensional plane-stress elasticity problem. The numerical results indicate that the integrated local Petrov–Galerkin sinc method can provide greater accuracy than the sinc method based on Interpolation of highest derivative. For the two example problems studied, the method's high rate of convergence can provide greater accuracy of stresses for the same computational cost as a displacement-based C^0-continuous and a mixed finite element. However, the still in development integrated local Petrov–Galerkin sinc method suffers from requiring a more fully populated stiffness matrix and relatively high computational cost of the matrix factorization.

Nomenclature

E	=	Young's modulus for isotropic material, MPa
$\mathbf{f}$	=	force vector
G	=	shear modulus for isotropic material, MPa
H^1	=	Hilbert space of order one
h	=	sinc mesh size in the τ domain
$\mathbf{K}$	=	stiffness matrix
N	=	sinc discretization parameter
n	=	number of sinc points along each computational axis, $n = 2N + 1$
$\bar{Q}_{ij}$	=	plane-stress reduced stiffness matrix
t, τ	=	physical and transformed domains, respectively, for sinc approximation
t_i	=	traction tensor, MPa
$\mathbf{u}$	=	global unknown vector
$\tilde{u}_i$	=	prescribed, nonhomogeneous displacement tensor, m
u_i	=	displacement vector, m
W^I	=	weight function of the Ith subdomain
$\mathbf{X}$	=	vector of coordinate location
x_1, x_2	=	orthogonal coordinate basis of the physical domain, m
β	=	penalty parameter
δW_{ext}	=	external virtual work
δW_{int}	=	internal virtual work
ϵ_{ij}	=	infinitesimal strain tensor
Γ	=	boundary of the domain Ω
Γ_u, Γ_t	=	portions of the boundary of the domain Ω on which essential and natural boundary conditions are applied
λ	=	Lagrange multiplier
ν	=	Poisson's ratio for isotropic material
ξ, η	=	orthogonal coordinate basis of computational domain
σ_{ij}	=	Cauchy stress tensor, MPa
$\phi(t)$, $\psi(\tau)$	=	mapping functions between t and τ domains
Ω	=	domain of boundary-value problem in physical domain

Subscript

$,xy$	=	partial differentiation with respect to x and y, $\partial^2(\cdot)/(\partial x \partial y)$

Presented as Paper 2392 at the 50th AIAA/ASME/ASCE/AHS/ASC Structures, Structural Dynamics, and Materials Conference, Palm Springs, CA, 4–7 May 2009; received 8 June 2009; revision received 26 January 2010; accepted for publication 23 February 2010.

*National Defense Science and Engineering Graduate (NDSEG) Research Fellow, Aerospace and Ocean Engineering, Sensors and Structural Health Monitoring Group. Student Member AIAA.

†Mitchell Professor, Aerospace and Ocean Engineering, Sensors and Structural Health Monitoring Group. Associate Fellow AIAA.

‡Postdoctoral Fellow, Aerospace and Ocean Engineering. Member AIAA.

I. Introduction

IN RECENT years, sinc approximation has been a highly studied topic in the research literature, particularly in conjunction with methods for numerical integration and solving two-point boundary-value problems (BVPs). Sinc approximation has been used as the basis function in both the sinc-collocation method and the sinc–Galerkin method because of the ease with which it may handle the presence of singularities or unbounded domains [1]. Furthermore, the sinc function is highly effective at capturing oscillating behavior in space and is thus quite useful for solutions with such characteristics.

Difficulties in the sinc-collocation method arise in applying the method to a BVP with mixed, Neumann-type, boundary conditions because the derivatives of the sinc functions at the boundaries are undefined [2]. Narasimhan et al. [3] used the finite difference method to calculate the derivatives of the dependent variables near the boundaries. Wu et al. [2] addressed this issue by introducing a sinc-collocation method with boundary treatment, which they showed to provide good convergence and easy treatment of the boundary conditions.

Much attention has been given to the sinc–Galerkin method, and its efficiency has been proved for both linear and nonlinear BVPs [4–7]. Al-Khaled [8] compared the sinc–Galerkin method with He's [9,10] homotopy perturbation method for singular two-point BVPs. El-Gamel [11] applies the sinc–Galerkin method to a fifth-order BVP and compares the results with sixth-degree B-spline functions.

The results of El-Gamel's study [11] indicate that the sinc–Galerkin generally performs better than the B-spline approach.

The traditional finite element method, the sinc–Galerkin and sinc-collocation methods, and most meshless methods approximate the primary variables through interpolation and the derivatives of the basis functions are computed. With such methods, errors in the primary variable are amplified through differentiation. However, using integration results in smoothing of these inherent errors. This philosophy is employed by the procedure of indirect or integrated radial basis function networks (IRBFN) by Mai-Duy and Tran-Cong [12,13], by Wu and Ren's [14] differential quadrature method based on the highest derivative (DQIHD), and by Li and Wu's [15] sinc method based on interpolation of highest derivatives (SIHD). All three of these methods rely on interpolation of the highest-order derivative and a subsequent integration of this representation to obtain the unknown function. DQIHD uses analytic integration of Lagrange interpolation polynomials to perform the integration. SIHD uses numerical indefinite integration based on the double-exponential transformation as developed by Muhammad and Mori [16] to efficiently perform the integration. Both of these techniques are collocation methods.

The IRBFN approach has been studied extensively. Mai-Duy and Tran-Cong [12] proposed both the direct or differentiated and indirect or integrated radial basis function networks (DRBFN and IRBFN, respectively) for approximation of functions. They used the IRBFN basis function in the collocation method and showed it to provide greater accuracy than the DRBFN used with collocation method [17]. Mai-Duy and Tran-Cong [18] also used the IRBFN with the weak form of the governing equation in a Galerkin formulation; however, the natural boundary conditions were still imposed as with the collocation scheme. Their results indicated that the Galerkin procedure exhibited greater accuracy and higher rates of convergence than by the collocation scheme. Furthermore, they noted that the IRBFN basis function maintained a lower matrix condition number than the DRBFN approach.

The differential quadrature method (DQM) was first introduced by Bellman and Casti [19]. Substantial work has been done [20–24] to apply the DQM method for structural mechanics problems; however, to our knowledge, no additional work has been done implementing the integrated form, the DQIHD method, since its recent introduction. We emphasize that SIHD and DQIHD are collocation methods and require satisfying both natural and essential boundary conditions [14,15,25,26].

Slemp and Kapania [25,26] showed SIHD to be an appropriate tool for computation of through-the-thickness interlaminar stresses in laminated composite and functionally graded composites. Typically, BVPs in structural mechanics are expressed in terms of displacements and strains are computed from derivatives of displacements. Because the highest derivative in the governing equation is the primary unknown in SIHD, the necessary derivatives for interlaminar stress computation are obtained without postprocessing.

A recent review of meshless methods was provided by Nguyen et al. [27]. They note that meshless method are typically implemented either by the collocation method or by Petrov–Galerkin or Bubnov–Galerkin methods. The meshless local Petrov–Galerkin (MLPG) method serves as the basis for domain decomposition in many meshless methods [28]. Batra and Zhang [29] compare collocation and the MLPG method implemented with the symmetric smoothed particle hydrodynamics (SSPH) basis function for two-dimensional static structural mechanics problems. Their results indicate the MLPG method provides greater accuracy than the collocation method with the SSPH basis function.

In this paper, we develop a new approximate method for solving elliptic boundary-value problems by using basis functions obtained by indefinite integration based on the double-exponential transformation [30]. The method follows the philosophy of the meshless local Petrov–Galerkin method; however, the particles or sinc points must lie in a set pattern on a rectangular grid as prescribed by the double-exponential transformation. Thus, it is not a meshless method. Moreover, the use of double-exponential indefinite integration distinguishes the approach from most methods that are differentiation based. The present method, like SIHD, DQIHD, and IRBFN, is called *integrated* because we first approximate the highest derivative in the weak form and use numerical indefinite integration based on the double-exponential transformation to obtain the lower derivatives and unknown function. The process of numerical indefinite integration is based on analytic integration of a sinc series interpolation of an integrand. Thus, the name integrated local Petrov–Galerkin sinc method is appropriate, as it classifies the method quite well. The unknowns in our approximation are the highest derivative in the weak form of the governing equation at each sinc point and constants of integration. To our knowledge, the method is a novel use of indefinite integration based on the double-exponential transformation and the meshless local Petrov–Galerkin method. The scope of this paper shall be to fully introduce the novel method, demonstrate the application of the method, and examine the accuracy and convergence properties for an example one- and two-dimensional elliptic boundary-value problem in structural mechanics.

The remainder of this paper is arranged as follows. Section I is the Introduction. In Sec. II, we review the process of indefinite integration by double-exponential transformation as used to develop the basis functions. Section III introduces the integrated local Petrov–Galerkin sinc method (ILPGSM). We present our results for a fixed–fixed tapered axial bar in Sec. IV. In Sec. V, we use the ILPGSM to solve the two-dimensional idealized Timoshenko cantilever beam problem. Finally, our conclusions are summarized.

II. Basis Functions Employing Double-Exponential Indefinite Integration

Muhammad and Mori [16] developed a method of numerical indefinite integration based on the double-exponential (DE) transformation. The method is called numerical indefinite integration because the value of the antiderivative of a function is found at a series of points, given the value of the function at those discrete points. The approach was used by Muhammad et al. [31] for solving integral equations by the sinc-collocation method, and the development is essential to the sinc method based on interpolation of highest derivative as presented in [15,25,26]. We also refer the readers to [32,33] for a good background on numerical integration using the DE transformation. We will review the concept as implemented in the ILPGSM.

The DE transformation was proposed by Takahasi and Mori [30] in 1973 for the evaluation of integrals of an analytic functions with endpoint singularities. One such DE transformation suggested by Sugihara and Matsuo [34] is

$$t = \psi(\tau) = \frac{1}{2}\tanh\left(\frac{\pi}{2}\sinh(\tau)\right) + \frac{1}{2} \tag{1}$$

There are two salient features exploited in sinc approximate methods. First, the domain is expanded from $t \in (0,1)$ to $\tau \in (-\infty, \infty)$. Second, the product $f(\psi(\tau))\psi'(\tau)$ decays double exponentially on the real line.

A function may be interpolated on $t \in (0,1)$ by a sinc cardinal series exploiting the DE transformation:

$$f(t) \approx \sum_{j=-N}^{N} f(\psi(jh))\mathrm{sinc}\left(\frac{\phi(t)}{h} - j\right) \tag{2}$$

where $\tau = \phi(t)$ is the inverse mapping of the DE transformation, $t = \psi(\tau)$, h is the sinc mesh size or point-spacing within the $\tau \in (-\infty, \infty)$ domain, and the sinc function is defined by $\mathrm{sinc}(t) = \sin(\pi t)/(\pi t)$. Figure 1 indicates the discretized mapping between the t and τ domains.

Consider evaluation of an integral

$$\int_0^s f(t)\,\mathrm{d}t$$

for $0 \le s \le 1$. The integrand is transformed to the $\tau \in (-\infty, \infty)$ domain. We may write

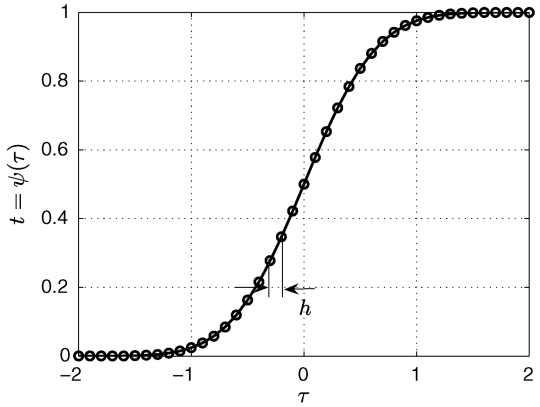

Fig. 1 Domain mapping between t and τ domains via Eq. (1).

$$\int_0^s f(t)\,\mathrm{d}t = \int_{-\infty}^{\phi(s)} f(\psi(\tau))\psi'(\tau)\,\mathrm{d}\tau \tag{3}$$

Now $f(\psi(\tau))\psi'(\tau)$ may be expanded employing the sinc series approximation:

$$f(\psi(\tau))\psi'(\tau) = \sum_{j=-N}^{N} f(\psi(jh))\psi'(jh)\mathrm{sinc}\left(\frac{\tau}{h} - j\right) \tag{4}$$

Substituting Eq. (4) into the integrand of Eq. (3) we obtain

$$\int_0^s f(t)\,\mathrm{d}t = h\sum_{j=-N}^{N} f(\psi(jh))\psi'(jh)\left(\frac{1}{2} + \frac{1}{\pi}\mathrm{Si}\left(\frac{\pi\phi(s)}{h} - \pi j\right)\right) \tag{5}$$

which holds for all $s \in [0, 1]$, where $\mathrm{Si}(x)$ is the sine integral function [35] defined by

$$\mathrm{Si}\,(x) = \int_0^x \sin(s)/s\,\mathrm{d}s$$

Muhammad et al. [31] note that the convergence rate to be of order $(\log(N)/N)\exp(-c_1 N/\log(c_2 N))$ for some positive c_1 and c_2.

It should be noted that evaluating the sine integral is not trivial. MATLAB offers a function SININT as part of its special functions. However, inspecting the m-file reveals that symbolic math is used to perform the operation. Numerical experiment has revealed that the SININT function will take 42 s to perform the operation just 5000 times on a 1.61 GHz, Windows XP PC with 2 GB of RAM. There are both trig and polynomial series expansions for the sine integral; however, the trig series is divergent for $x \gg 1$ and the polynomial series is slowly convergent and not precise for $x \gg 1$ [35]. Recently, an algorithm for rational approximation of the sine and cosine integrals was developed by MacLeod [36]. Although MacLeod [36] provides the algorithm via the NUMERALGO section of NETLIB, the algorithm was implemented by the authors in MATLAB for the present study. The same 5000 operations using the rational approximation of MacLeod runs in only 0.015 s on the same PC, 2800 times faster than MATLAB's SININT function.

A. First-Order Approximation with Sinc Interpolation (Sinc-1)

In this paper, we consider only second-order boundary-value problems. The weak form for such a problem contains the first-order derivatives, and thus the basis functions must be able to be evaluated up to the first-order derivatives.

1. One-Dimensional Problems

We assume that $f'(\xi_i)$ is known for all ξ_i such that $0 < \xi_i < 1$ and corresponding to $\xi_i = \psi(ih)$ with

$$i = \{-N, -N+1, \ldots, -1, 0, 1, \ldots, N-1, N\}$$

The derivative $f'(\xi_i)$ may be interpolated using a sinc series:

$$f'(\xi) = \sum_{j=-N}^{N} f'(\xi_j)\mathrm{sinc}\left(\frac{\phi(\xi)}{h} - j\right) \tag{6}$$

Employing the previously mentioned method of indefinite integration, we may write the function at a given point ξ by

$$f(\xi) = \sum_{j=-N}^{N} f'(\xi_j)h\psi'(jh)\left[\frac{1}{2} + \frac{1}{\pi}\mathrm{Si}\left(\frac{\pi\phi(\xi)}{h} - \pi j\right)\right] + C$$

We can express both of these relations in matrix form by

$$f'(\xi) = \mathbf{E}(\xi)\mathbf{u}, \qquad f(\xi) = \mathbf{A}(\xi)\mathbf{u} \tag{7}$$

where

$$\mathbf{u} = \{f'(x_{-N}), f'(x_{-N+1}), \ldots, f'(x_N), C\}^T$$

and appropriate definition of $\mathbf{E}(\xi)$ and $\mathbf{A}(\xi)$ [37].

2. Two-Dimensional Problems

For a two-dimensional problem, assume $f_{,\xi\eta}(\xi_i, \eta_j)$ is known and can be accurately interpolated using a tensor product of sinc series along each coordinate axis:

$$f_{,\xi\eta}(\xi, \eta) = \sum_{i=-N}^{N}\sum_{j=-N}^{N} f_{,\xi\eta}(\xi_i, \eta_j)\left[\mathrm{sinc}\left(\frac{\phi(\xi)}{h} - i\right)\right] \times \left[\mathrm{sinc}\left(\frac{\phi(\eta)}{h} - j\right)\right] \tag{8}$$

Employing the indefinite integration on ξ and applying Eq. (5), we write

$$f_{,\eta}(\xi, \eta) = \sum_{i=-N}^{N}\sum_{j=-N}^{N} f_{,\xi\eta}(\xi_i, \eta_j)\left\{h\psi'(ih)\left[\frac{1}{2} + \frac{1}{\pi}\mathrm{Si}\left(\frac{\pi\phi(\xi)}{h} - \pi i\right)\right]\right\}\left[\mathrm{sinc}\left(\frac{\phi(\eta)}{h} - j\right)\right] + C_1(\eta) \tag{9}$$

Note that in Eq. (9), $C_1(\eta)$ is a function of η only. We approximate this function by the sinc series of the form

$$C_1(\eta) = \sum_{j=-N}^{N} C_1(\eta_j)\mathrm{sinc}\left(\frac{\phi(\eta)}{h} - j\right) \tag{10}$$

Thus, Eq. (9) becomes

$$f_{,\eta}(\xi, \eta) = \sum_{i=-N}^{N}\sum_{j=-N}^{N} f_{,\xi\eta}(\xi_i, \eta_j)T_2(\xi, i)T_1(\eta, j) + \sum_{j=-N}^{N} C_1(\eta_j)T_1(\eta, j) \tag{11}$$

where

$$T_1(\xi, j) = \mathrm{sinc}\left(\frac{\phi(\xi)}{h} - j\right) \tag{12}$$

$$T_2(\xi, j) = h\psi'(jh)\left[\frac{1}{2} + \frac{1}{\pi}\mathrm{Si}\left(\frac{\pi\phi(\xi)}{h} - \pi j\right)\right] \tag{13}$$

Similarly, we write

$$f_{,\xi}(\xi, \eta) = \sum_{j=-N}^{N}\sum_{i=-N}^{N} f_{,\xi\eta}(\xi_i, \eta_j)T_1(\xi, i)T_2(\eta, j) + \sum_{i=-N}^{N} C_2(\xi_i)T_1(\xi, i) \tag{14}$$

The indefinite integration is performed on Eqs. (11) and (14) yielding

$$f(\xi,\eta)=\int f_{,\eta}(\xi,\eta)\,\mathrm{d}\eta=\int\Bigg(\sum_{i=-N}^{N}\sum_{j=-N}^{N}f_{,\xi\eta}(\xi_i,\eta_j)T_2(\xi,i)T_1(\eta,j)+\sum_{j=-N}^{N}C_1(\eta_j)T_1(\eta,j)\Bigg)\mathrm{d}\eta+\tilde{C}_3(\xi)+\tilde{C}_4 \tag{15a}$$

$$f(\xi,\eta)=\int f_{,\xi}(\xi,\eta)\,\mathrm{d}\xi=\int\Bigg(\sum_{i=-N}^{N}\sum_{j=-N}^{N}f_{,\xi\eta}(\xi_i,\eta_j)T_1(\xi,i)T_2(\eta,j)+\sum_{i=-N}^{N}C_2(\xi_i)T_1(\xi,i)\Bigg)\mathrm{d}\xi+\tilde{C}_5(\eta)+\tilde{C}_6 \tag{15b}$$

Simplifying, we obtain

$$f(\xi,\eta)=\int f_{,\eta}(\xi,\eta)\,\mathrm{d}\eta=\sum_{i=-N}^{N}\sum_{j=-N}^{N}f_{,\xi\eta}(\xi_i,\eta_j)T_2(\xi,i)T_2(\eta,j)+\sum_{j=-N}^{N}C_1(\eta_j)T_2(\eta,j)+\tilde{C}_3(\xi)+\tilde{C}_4 \tag{16a}$$

$$f(\xi,\eta)=\int f_{,\xi}(\xi,\eta)\,\mathrm{d}\xi=\sum_{i=-N}^{N}\sum_{j=-N}^{N}f_{,\xi\eta}(\xi_i,\eta_j)T_2(\xi,i)T_2(\eta,j)+\sum_{i=-N}^{N}C_2(\xi_i)T_2(\xi,i)+\tilde{C}_5(\eta)+\tilde{C}_6 \tag{16b}$$

By reconciling the two expressions for $f(\xi,\eta)$, it is clear that

$$\tilde{C}_3(\xi)=\sum_{i=-N}^{N}C_2(\xi_i)T_2(\xi,i),\qquad \tilde{C}_5(\eta)=\sum_{j=-N}^{N}C_1(\eta_j)T_2(\eta,j)$$
$$\tilde{C}_4=\tilde{C}_6=C_3 \tag{17}$$

where C_3 is an arbitrary constant of integration. Therefore, $f(\xi,\eta)$ may be expressed by

$$f(\xi,\eta)=\sum_{i=-N}^{N}\sum_{j=-N}^{N}f_{,\xi\eta}(\xi_i,\eta_j)T_2(\xi,i)T_2(\eta,j)+\sum_{j=-N}^{N}C_1(\eta_j)T_2(\eta,j)+\sum_{i=-N}^{N}C_2(\xi_i)T_2(\xi,i)+C_3 \tag{18}$$

Now we introduce the global unknown vector $\mathbf{u}=\{\mathbf{f}_{,\xi\eta},\mathbf{C}_1,\mathbf{C}_2,C_3\}^T$, where

$$\mathbf{C}_1=\{C_1(\xi_{-N}),C_1(\xi_{-N+1}),\ldots,C_1(\xi_N)\}$$

$$\mathbf{C}_2=\{C_2(\eta_{-N}),C_2(\eta_{-N+1}),\ldots,C_2(\eta_N)\}$$

and

$$\mathbf{f}_{,\xi\eta}=\{f_{,\xi\eta}(\xi_{-N},\eta_{-N}),f_{,\xi\eta}(\xi_{-N+1},\eta_{-N}),\ldots,f_{,\xi\eta}(\xi_N,\eta_{-N})\ f_{,\xi\eta}(\xi_{-N},\eta_{-N+1}),\ldots,f_{,\xi\eta}(\xi_N,\eta_N)\}$$

The basis functions may be written in matrix form. Accordingly, we may say

$$f_{,\xi}(\xi,\eta)=\mathbf{A}_1(\xi,\eta)\mathbf{u},\qquad f_{,\eta}(\xi,\eta)=\mathbf{A}_2(\xi,\eta)\mathbf{u}$$
$$f(\xi,\eta)=\mathbf{B}(\xi,\eta)\mathbf{u} \tag{19}$$

where $\mathbf{A}_1$, $\mathbf{A}_2$, and $\mathbf{B}$ were defined by Slemp et al. [37]. This basis function will be referred to as the sinc-1 basis function.

B. Second-Order Approximation with Sinc Interpolation (Sinc-2)

The sinc interpolation given by Eq. (2) may exhibit significant oscillations. However, the integrated expression in Eq. (5) varies smoothly between points. For this reason, we would expect our results to be better if we expand the second-order derivatives. In doing so, neither $f_{,\xi}$ nor $f_{,\eta}$ are interpolated by the sinc interpolation of Eq. (2).

1. *One-Dimensional Problems*

We approximate the second derivative using a sinc series:

$$f''(\xi)=\sum_{j=-N}^{N}f''(\xi_j)\mathrm{sinc}\left(\frac{\phi(\xi)}{h}-j\right) \tag{20}$$

where we assume that $f''(\xi_j)$ is known for all ξ_j such that $0<\xi_j<1$ and corresponding to $\xi_j=\psi(jh)$ with

$$j=\{-N,-N+1,\ldots,-1,0,1,\ldots,N-1,N\}$$

Employing the indefinite integration scheme, we write the first derivative by

$$f'(\xi)=\sum_{j=-N}^{N}f''(\xi_j)h\psi'(jh)\left[\frac{1}{2}+\frac{1}{\pi}\mathrm{Si}\left(\frac{\pi\phi(\xi)}{h}-\pi j\right)\right]+C_1 \tag{21}$$

We can write $f'(\xi_j)$ (the first derivative, evaluated at the sinc points) and repeat the integration process to obtain the function itself:

$$f(\xi)=\sum_{i=-N}^{N}\sum_{j=-N}^{N}h^2\psi'(ih)\psi'(jh)\left[\frac{1}{2}+\frac{1}{\pi}\mathrm{Si}\left(\frac{\pi\phi(\xi)}{h}-\pi i\right)\right]\times\left[\frac{1}{2}+\frac{1}{\pi}\mathrm{Si}(\pi(i-j))\right]f''(\xi_j)+C_1\xi+C_2 \tag{22}$$

We can write this in matrix form by Eq. (7) with new definitions for $\mathbf{E}$ and $\mathbf{A}$ as given in Slemp et al. [37].

2. *Two-Dimensional Problems*

We approximate $f_{,\xi\xi\eta\eta}(\xi,\eta)$ by a sinc series in two dimensions. Applying the indefinite integration rule as before, the necessary lower-order derivatives are given by

$$f_{,\xi}(\xi,\eta)=\sum_{i=-N}^{N}\sum_{j=-N}^{N}T_2(\xi,i)T_3(\eta,j)f_{,\xi\xi\eta\eta}(\xi_i,\eta_j)+\sum_{j=-N}^{N}C_1(\eta_j)T_3(\eta,j)+\sum_{i=-N}^{N}[C_2(\xi_i)T_2(\xi,i)\eta+C_4(\xi_i)T_2(\xi,i)]+C_5\eta+C_6 \tag{23}$$

$$f_{,\eta}(\xi,\eta)=\sum_{i=-N}^{N}\sum_{j=-N}^{N}T_3(\xi,i)T_2(\eta,j)f_{,\xi\xi\eta\eta}(\xi_i,\eta_j)+\sum_{i=-N}^{N}C_2(\xi_i)T_3(\xi,i)+\sum_{j=-N}^{N}[C_1(\eta_j)T_2(\eta,j)\xi+C_3(\eta_j)T_2(\eta,j)]+C_5\xi+C_7 \tag{24}$$

$$f(\xi,\eta)=\sum_{i=-N}^{N}\sum_{j=-N}^{N}T_3(\xi,i)T_3(\eta,j)f_{,\xi\xi\eta\eta}(\xi_i,\eta_j)+\sum_{i=-N}^{N}[C_1(\eta_j)T_3(\eta,j)\xi+C_3(\eta_j)T_3(\eta,j)]+\sum_{i=-N}^{N}[C_2(\xi_i)T_3(\xi,i)\eta+C_4(\xi_i)T_3(\xi,i)]+C_5\xi\eta+C_6\xi+C_7\eta+C_8 \tag{25}$$

where

$$T_3(\xi,j)=\sum_{i=-N}^{N}h^2\psi'(ih)\psi'(jh)\left[\frac{1}{2}+\frac{1}{\pi}\mathrm{Si}\left(\frac{\pi\phi(\xi)}{h}-\pi i\right)\right]\times\left[\frac{1}{2}+\frac{1}{\pi}\mathrm{Si}(\pi(i-j))\right] \tag{26}$$

To write the basis functions in matrix form, we introduce the global unknown vector:

$$\mathbf{u}=\{\mathbf{f}_{,\xi\xi\eta\eta},\mathbf{C}_1,\mathbf{C}_2,\mathbf{C}_3,\mathbf{C}_4,C_5,C_6,C_7,C_8\}^T$$

where

$$\mathbf{C}_1=\{C_1(\xi_{-N}),C_1(\xi_{-N+1}),\ldots,C_1(\xi_N)\}$$

and with similar definitions for $\mathbf{C}_2$, $\mathbf{C}_3$, and $\mathbf{C}_4$ and with

$$\mathbf{f}_{,\xi\xi\eta\eta}=\{f_{,\xi\xi\eta\eta}(\xi_{-N},\eta_{-N}),f_{,\xi\xi\eta\eta}(\xi_{-N+1},\eta_{-N}),\ldots,f_{,\xi\xi\eta\eta}(\xi_N,\eta_{-N}) f_{,\xi\xi\eta\eta}(\xi_{-N},\eta_{-N+1}),\ldots,f_{,\xi\xi\eta\eta}(\xi_N,\eta_N)\}$$

Thus, in matrix form, the basis function is given by Eq. (19) with the appropriate definition of $\mathbf{A}_1$, $\mathbf{A}_2$, and $\mathbf{B}$ [37]. This basis function is referred to as the sinc-2 basis function.

C. First-Order Approximation with Linear Interpolation (Linear)

Now we develop our third type of basis function, which uses the double-exponential integration method to obtain values of the function at the sinc points (ξ_i,η_j). Between these points, both the first derivative and the function are linearly interpolated. Because we do not use the sinc interpolation but rather linear interpolation, the first-order derivatives may be approximated without introducing oscillations. For a one-dimensional problem, we evaluate Eq. (7) only at each sinc point. For two dimensions, Eq. (19) is evaluated only at each sinc point. Between sinc points, both the first derivatives and the function are linearly interpolated from that at the surrounding sinc points. This may be performed by

$$f(\mathbf{X})=\sum_{i=1}^{n_e}N_i(\mathbf{X})f(\mathbf{X}_i) \tag{27}$$

where $\mathbf{X}$ is the coordinates of the point of interest, n_e is the number of surrounding points to be interpolated between ($n_e=2$ for 1-D, $n_e=4$ for 2-D), $N_i(\mathbf{X})$ are the Lagrange interpolation polynomials evaluated at the point of interest, and $f(\mathbf{X}_i)$ are the function values evaluated at the surrounding sinc points.

This basis function is referred to as the linear basis function.

III. Formulation of Two-Dimensional Elastostatic Problems

To develop the ILPGSM, we consider plane-stress elasticity on the domain Ω with boundary Γ (see Fig. 2). To develop the governing equations, the principle of virtual work is employed. The internal and external virtual work are given by

$$\delta W_{\mathrm{int}}=\int_\Omega(\sigma_{11}\delta\epsilon_{11}+\sigma_{12}\delta\gamma_{12}+\sigma_{22}\delta\epsilon_{12})\,\mathrm{d}\Omega \tag{28}$$

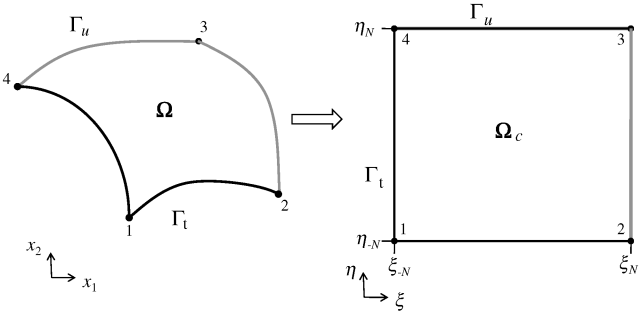

Fig. 2 Diagram of physical and computational domain.

$$\delta W_{\mathrm{ext}}=\int_\Gamma(t_1\delta u_1+t_2\delta u_2)\,\mathrm{d}\Gamma \tag{29}$$

where u_i is the displacement vector, σ_{ij} is the stress tensor, and t_i is a vector representing the traction applied to the edge Γ $(i,j=1,2)$. Note that $\Gamma=\{\mathbf{X}:\mathbf{X}\in\Gamma_u\cup\Gamma_t\}$, where Γ_u and Γ_t are portions of the boundary in which an applied displacement and traction are imposed, respectively.

The constitutive relation for linearly elastic isotropic material in the plane-stress condition is given by

$$\begin{Bmatrix}\sigma_{11}\\ \sigma_{22}\\ \sigma_{12}\end{Bmatrix}=\begin{bmatrix}\bar{Q}_{11}&\bar{Q}_{12}&0\\ \bar{Q}_{12}&\bar{Q}_{22}&0\\ 0&0&\bar{Q}_{66}\end{bmatrix}\begin{Bmatrix}\epsilon_{11}\\ \epsilon_{22}\\ \gamma_{12}\end{Bmatrix} \tag{30}$$

where the plane-stress reduced stiffnesses are defined such that $\bar{Q}_{11}=\bar{Q}_{22}=E/(1-\nu^2)$, $\bar{Q}_{12}=\nu\bar{Q}_{11}$, and $\bar{Q}_{66}=G$. The infinitesimal strains are defined by

$$\{\epsilon_{11},\epsilon_{22},\gamma_{12}\}^T=\{u_{1,1},u_{2,2},u_{1,2}+u_{2,1}\}^T \tag{31}$$

The balance of internal and external virtual work, expressed in terms of displacements and their variations, is written as

$$\int_\Omega(\bar{Q}_{11}u_{1,1}+\bar{Q}_{12}u_{2,2})\delta u_{1,1}+\bar{Q}_{66}(u_{1,2}+u_{2,1})\delta u_{1,2}+(\bar{Q}_{22}u_{2,2}+\bar{Q}_{12}u_{1,1})\delta u_{2,2}+\bar{Q}_{66}(u_{1,2}+u_{2,1})\delta u_{2,1}\,\mathrm{d}\Omega=\int_\Gamma t_1\delta u_1+t_2\delta u_2\,\mathrm{d}\Gamma \tag{32}$$

In the fashion of the MLPG method, the variations of displacements are independently selected to be a weight function with a compact support, $W^I(\mathbf{X})$, where I identifies the Ith support domain. Therefore, the equilibrium equation (32) becomes a system of equations, each with the following form:

$$\begin{aligned}&\int_{\Omega_I}(\bar{Q}_{11}u_{1,1}+\bar{Q}_{12}u_{2,2})W^I_{,1}(\mathbf{X})+\bar{Q}_{66}(u_{1,2}+u_{2,1})W^I_{,2}(\mathbf{X})\,\mathrm{d}\Omega_I\\ &\quad=\int_{\Gamma_I}t_1W^I(\mathbf{X})\,\mathrm{d}\Gamma_I\\ &\int_{\Omega_I}(\bar{Q}_{22}u_{2,2}+\bar{Q}_{12}u_{1,1})W^I_{,2}(\mathbf{X})+\bar{Q}_{66}(u_{1,2}+u_{2,1})W^I_{,1}(\mathbf{X})\,\mathrm{d}\Omega_I\\ &\quad=\int_{\Gamma_I}t_2W^I(\mathbf{X})\,\mathrm{d}\Gamma_I\end{aligned} \tag{33}$$

where Ω_I is the support of weight function W^I, $\Gamma=\{\mathbf{X}:\mathbf{X}\in\Omega_I\cap\Gamma\}$, and $u_i(\mathbf{X})$ and their derivatives are approximated by the previously introduced basis functions. The weight functions are selected such that $W^I\in H^1$ and $W^I(\mathbf{X})>0$ for $\mathbf{X}\in\Omega_I$ and such that $W^I(\mathbf{X})=0$ for $\mathbf{X}\notin\Omega_I$.

A. Domain Transformation

The physical domain is transformed to a rectangular computational domain defined by

$$\Omega_c = \{\mathbf{X}_c = (\xi, \eta) : (\xi_{-N} \le \xi \le \xi_N) \cap (\eta_{-N} \le \eta \le \eta_N)\}$$

where (ξ_i, η_j) are sinc points, distributed by the double-exponential transformation. For a mesh size h, the sinc points correspond to

$$i, j = \{-N, -N+1, \ldots, -1, 0, 1, \ldots N-1, N\}$$

defined by $\xi_i = \psi(ih)$ and $\eta_j = \psi(jh)$ [see Eq. (1)]. There are a total of $n = 2N + 1$ sinc points along each axis. The domain transformation between the physical and computational domain is performed using a mapping of the form $x_1 = f_1(\xi, \eta)$ and $x_2 = f_2(\xi, \eta)$. We suggest using Lagrange interpolation polynomials to represent the geometric transformation in a similar manner to the isoparametric elements in the finite element method [38,39]; however, any generic angle preserving mapping is applicable. The primary displacement variables and their pertinent derivatives in the physical and computational domain are related by

$$u_i(x_1, x_2) = \bar{u}_i(\xi, \eta), \qquad \frac{\partial u_i}{\partial x_j}(x_1, x_2) = \frac{\partial \bar{u}_i}{\partial \xi}\frac{\partial \xi}{\partial x_j} + \frac{\partial \bar{u}_i}{\partial \eta}\frac{\partial \eta}{\partial x_j} \quad (34)$$

where $i, j = 1, 2$ and variables with an overbar are expressed in the computational domain. We note that the weight functions $W^I(\mathbf{X})$ may be related to those expressed in the computational domain, $\bar{W}^I(\mathbf{X}_c)$, by Eq. (34) as well.

The area $\mathrm{d}\Omega_I$ is mapped into the computational domain by

$$\mathrm{d}\,\Omega_I = \left(\frac{\partial f_1}{\partial \xi}\frac{\partial f_2}{\partial \eta} - \frac{\partial f_1}{\partial \eta}\frac{\partial f_2}{\partial \xi}\right)\mathrm{d}\xi\mathrm{d}\eta, \qquad \mathrm{d}\Omega_I = |J|\mathrm{d}\xi\mathrm{d}\eta \quad (35)$$

We note that in the computational domain, each edge of the boundary Γ_c corresponds to either constant ξ or constant η. Therefore, the boundary integrals can be transformed to the computational domain by relating the differential line elements to differential changes in ξ or η:

$$\mathrm{d}\,\Gamma_{\xi=c} = \sqrt{\left(\frac{\partial f_1}{\partial \eta}\right)^2 + \left(\frac{\partial f_2}{\partial \eta}\right)^2}\,\mathrm{d}\eta$$

$$\mathrm{d}\Gamma_{\eta=c} = \sqrt{\left(\frac{\partial f_1}{\partial \xi}\right)^2 + \left(\frac{\partial f_2}{\partial \xi}\right)^2}\,\mathrm{d}\xi \quad (36)$$

where $\Gamma_{\xi=c}$ and $\Gamma_{\eta=c}$ are portions of boundary in the physical domain on which ξ and η are, respectively, constant in the computational domain. By defining the following matrices,

$$\mathbf{K}^I_{ij} = \int_{\Omega_I} W^I_{,i}\left(\frac{\partial \xi}{\partial x_j}\mathbf{A}_1(\xi, \eta) + \frac{\partial \eta}{\partial x_j}\mathbf{A}_2(\xi, \eta)\right)|J|\,\mathrm{d}\xi\,\mathrm{d}\eta \quad (37)$$

the local Petrov–Galerkin approximation can be written as

$$\begin{bmatrix} \bar{Q}_{11}\mathbf{K}^I_{11} + \bar{Q}_{66}\mathbf{K}^I_{22} & \bar{Q}_{12}\mathbf{K}^I_{12} + \bar{Q}_{66}\mathbf{K}^I_{21} \\ \bar{Q}_{12}\mathbf{K}^I_{21} + \bar{Q}_{66}\mathbf{K}^I_{12} & \bar{Q}_{12}\mathbf{K}^I_{22} + \bar{Q}_{66}\mathbf{K}^I_{11} \end{bmatrix}\begin{pmatrix} \bar{\mathbf{u}}_1 \\ \bar{\mathbf{u}}_2 \end{pmatrix} = \begin{pmatrix} \int_{\Gamma_I} t_1 W^I(\mathbf{X})\,\mathrm{d}\Gamma_I \\ \int_{\Gamma_I} t_2 W^I(\mathbf{X})\,\mathrm{d}\Gamma_I \end{pmatrix} \quad (38)$$

where $\bar{\mathbf{u}}_1$ and $\bar{\mathbf{u}}_2$ are the unknowns of the basis functions. By selecting n_u weight functions of compact support, where n_u is the number of unknowns per primary variable, an equal number of equations as unknowns are obtained. Because the sinc points are distributed such that they lie on a rectangular domain, we select weight functions with rectangular support as indicated in Fig. 3. We specify the support of the Ith weight function in the computational domain to be defined by

$$\Omega_{cI} = \{\mathbf{X}_c : (\xi_{\min} \le \xi \le \xi_{\max}) \cap (\eta_{\min} \le \eta \le \eta_{\max}) \cap \Omega_c\}$$

Traditionally, the MLPG method would select Gauss functions or other radial basis functions [29,40,41] as weights; however, for our study, we use weight functions having quadratic variations of the form

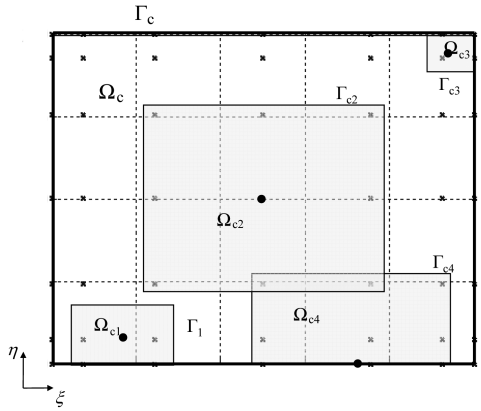

Fig. 3 Local Petrov–Galerkin subdomains in the computational domain. The dots indicate centers of the given subdomain; x indicates sinc points within the computational domain.

$$\bar{W}^I(\xi, \eta) = \begin{cases} (a^I_1\xi^2 + b^I_1\xi + c^I_1)(a^I_2\eta^2 + b^I_2\eta + c^I_2), & (\xi, \eta) \in \Omega_{cI} \\ 0, & (\xi, \eta) \in \Omega_{cI} \end{cases}$$

$$a^I_1 = \frac{-4}{(\xi_{\max} - \xi_{\min})^2}, \qquad b^I_1 = \frac{4(\xi_{\max} + \xi_{\min})}{(\xi_{\max} - \xi_{\min})^2}$$

$$c^I_1 = \frac{-4\xi_{\max}\xi_{\min}}{(\xi_{\max} - \xi_{\min})^2}, \qquad a^I_2 = \frac{-4}{(\eta_{\max} - \eta_{\min})^2}$$

$$b^I_2 = \frac{4(\eta_{\max} + \eta_{\min})}{(\eta_{\max} - \eta_{\min})^2}, \qquad c^I_2 = \frac{-4\eta_{\max}\eta_{\min}}{(\eta_{\max} - \eta_{\min})^2} \quad (39)$$

B. Essential Boundary Conditions

Because the basis functions do not possess the Kronecker delta property, applying the essential boundary conditions is not trivial. To do so, we implement two approaches: the traditional penalty method and the Lagrange multiplier method.

For the traditional penalty method, the local reaction forces given by

$$\int_{\Gamma_I} t_i \delta u_i\,\mathrm{d}\Gamma_I$$

are replaced by a penalty term for a subdomain intersecting the boundary on which the essential boundary conditions are imposed. That is, the local reaction forces are replaced by the following term:

$$\beta\int_{\Gamma_I}(u_i - \tilde{u}_i)\delta u_i\,\mathrm{d}\Gamma_I \quad (40)$$

where β is a penalty parameter. Zhu and Atluri [42] suggest a range of $(10^3$–$10^7)E$ for the penalty parameter, where E is the relative magnitude of the governing equations. For structures problems, we take E to be Young's modulus of the material. Because of the large penalty parameter β, the essential boundary conditions are imposed in an approximate sense.

The present method also uses the Lagrange multiplier approach. In this case, for a boundary on which an essential boundary condition is imposed, the local reaction force given by

$$\int_{\Gamma_I} t_i \delta u_i\,\mathrm{d}\Gamma_I$$

is replaced by

$$\lambda^I_i\int_{\Gamma_I}(\delta u_i)\,\mathrm{d}\Gamma_I + \int_{\Gamma_I}\delta\lambda^I_i(u - \tilde{u})\,\mathrm{d}\Gamma_I \quad (41)$$

where λ_i^I, is introduced as an additional unknown. Because $\delta\lambda_i^I$ are arbitrary, they are independently set to $\beta W^I(\mathbf{X})$ resulting in an additional equation in which β is included to provide a similar magnitude between equations resulting from $\delta\lambda_i^I$ and equations resulting from δu_i. In practice, $\lambda_i^I \int_{\Gamma_I} (\delta u_i)\, \mathrm{d}\Gamma_I$ need not be evaluated. This term can simply be lumped into the unknown λ_i^I. Furthermore, in order to maintain a similar magnitude of the unknowns and prevent ill conditioning, λ_i^I was normalized by β.

C. Integration Scheme

The integration in the weak form merits some discussion. For basis functions with sinc interpolation, we integrate over each subdomain using Gauss quadrature. Because the integrals involve expressions with sinc and sine integral functions, an exact quadrature rule cannot be used. To compensate, the number of integration points was increased until a similar result was obtained by two successive integration rules.

IV. One-Dimensional Tapered Axial Bar

To assess the accuracy of the ILPGSM, we perform one-dimensional, static analysis of a fixed–fixed, homogeneous, axial bar that is subjected to a uniform distributed force. The boundary-value problem is expressed by

$$[EA(x)u_{,1}(x)]_{,1} + p_0 = 0, \quad \text{in } \Omega = \{x{:}0 < x < L\}$$
$$u(0) = 0, \quad \text{and} \quad u(L) = 0$$

where E is Young's modulus, $A(x)$ is the cross-sectional area at a given x, and p_0 is the distributed force per unit length. Let A_0 represent the area at the root ($x = 0$). Accordingly, we normalize by introducing $\bar{u} = EA_0 u(x)/(p_0 L^2)$, $\bar{x} = x/L$, and $a(\bar{x}) = A(x)/A_0$. We drop the overbar. Note that the normalized stress is given by $\sigma = u_{,1}(x)$.

To obtain the local weak form, we multiply by a weight function of compact support, integrate over that support, and carry out the integration by parts. We obtain

$$W^I(x)a(x)u_{,1}(x)\big|_{x_{\min}^I}^{x_{\max}^I} - \int_{\Omega_I} (W_{,1}^I(x)a(x)u_{,1}(x) - W^I(x))\, \mathrm{d}\Omega_I = 0 \tag{42}$$

with $\Omega_I = \{x{:}x_{\min}^I \le x \le x_{\max}^I\}$.

The physical and computational domains are related by $x = (\xi - \xi_{-N})/(\xi_N - \xi_{-N})$. The displacement and its pertinent derivatives in the physical and computational domain are related in an analogous manner to the two-dimensional case presented in Sec. III. The primary variable and its derivative, $u(\xi)$ and $u_{,1}(\xi)$, are approximated by the basis functions. Note that by selecting n_u weight functions, Eq. (42) becomes a system of n_u equations of the form $\mathbf{Ku} = \mathbf{f}$. For the first-order basis functions, $n_u = n + 1$. For the second-order basis function, $n_u = n + 2$.

For the present study, weight functions of compact support were constructed by the following scheme. We select n_u weight functions whose subdomains are centered at $\xi_{I\text{-mid}}$ according to the DE transformation. For mesh size h, we select

$$\xi_{I\text{-mid}} = \phi\left(Nh\,\frac{2I - n_u - 1}{n_u - 1}\right), \qquad I = 1, 2, 3, \ldots, n_u$$

The subdomain widths are selected such that there are at least two sinc points within the subdomain. Let $\mathbf{x}$ be the vector of sinc points and let $\mathbf{x}_{\text{mid}}$ be the vector of subdomain centers; the function $\min 2(\mathbf{a})$

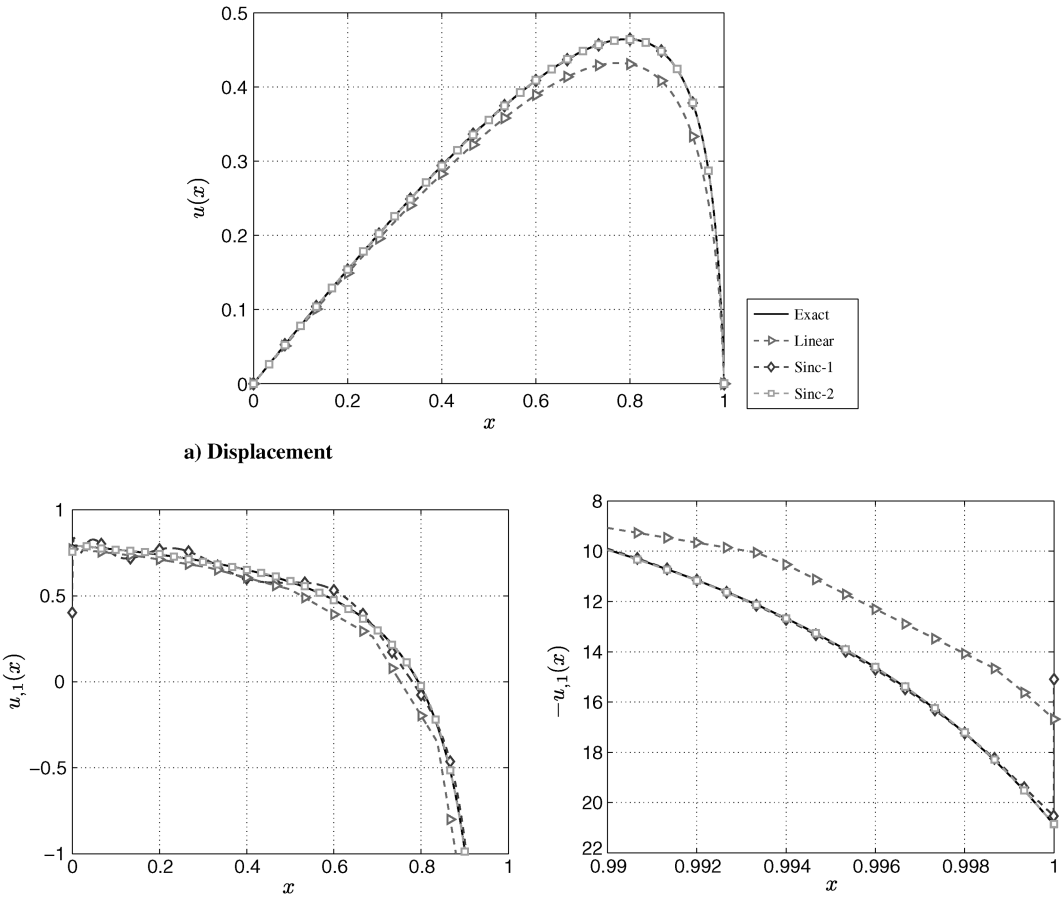

a) Displacement

b) Stress

c) Stress near the tip

Fig. 4 Displacement and stress obtained with $N = 10$ (21 sinc points) and the ILPGSM method using the Lagrange multiplier method to impose essential boundary conditions for $\delta = 0.01$. Results are compared with analytic solution.

returns the second-smallest entry in a vector **a**. Then the width of each subdomain is given by $d_I = 2\min 2(|\mathbf{x} - \mathbf{x}_{\text{sup}}|)$, the Ith subdomain maximum is given by $\xi_{\max} = \xi_{I\text{-mid}} + d_I/2$, and the Ith subdomain minimum is given by $\xi_{\min} = \xi_{I\text{-mid}} - d_I/2$. Note that there are some subdomains whose maximum or minimum lies outside of the domain Ω. The $\xi_{\min}$ and $\xi_{\max}$ are used in the one-dimensional equivalent to Eq. (39) to construct the weighting functions. However, the integration is performed over

$$\Omega_{cI} = \{\xi{:}(\xi_{\min} \leq \xi \leq \xi_{\max}) \cap (\xi \in \Omega_c)\}$$

The ILPGSM was implemented for the axial bar in MATLAB R14 Service Pack 2 using all three basis functions. The sinc mesh size h [see Eq. (2) and Fig. 1] was taken to be $2.5/N$. Slemp and Kapania [25] showed that choosing the mesh size $h = 2.5/N$ provides good accuracy and convergence for SIHD; therefore, it seems appropriate for the present study.

We consider a tapered bar with vanishing tip area. The area is selected having the form $a(x) = (1 - x + \delta)/(1 + \delta)$ with $\delta = 0.01$ and 0.0001, that is a linear area variation with root-to-tip area ratios of 101:1 and 10, 001:1, respectively. Our results were compared with the analytic solution (see Slemp et al. [37]):

$$u(x) = \frac{(\delta+1)(x\log(\delta) - (x-1)\log(\delta+1) - \log(-x+\delta+1))}{\log(\delta) - \log(\delta+1)}$$

In Fig. 4, we plot the solution obtained by the ILPGSM and the three basis functions using $N = 10$ for $\delta = 0.01$. For the ILPGSM results, the essential boundary conditions were imposed by the Lagrange multiplier method; however, similar results were obtained using the penalty method with a penalty parameter of 1×10^5. The figure indicates that the displacement and stress were predicted accurately using both the sinc-1 and sinc-2 basis functions. However, the displacement results obtained using the linear basis function are erroneous by 7% at its maximum and the stress results are erroneous by 29% at $x = L$. The sinc-1 basis function exhibits some oscillations in the stress, which is a characteristic of the sinc interpolation.

In Fig. 5, similar results were plotted for $\delta = 0.0001$ or a root-to-tip area ratio of 10, 001:1. For this case, both the sinc-1 and sinc-2 basis functions provide a very accurate approximation for displacement; however, the stress is only accurately approximated using the sinc-2 basis function. The linear basis function provides 13% error in maximum displacement and 41% error in the tip stress. The sinc-1 basis function exhibits substantial oscillations in the stress. The results obtained using the sinc-2 basis function are indistinguishable from the analytic solution. Despite the substantial stress concentration. Similar results were obtained using the penalty method to apply the essential boundary conditions with a similar level of accuracy.

To further numerically quantify the error, the following error norms are defined: one for the displacement, $\|\epsilon\|_0$, and one for the stress, $\|\epsilon\|_1$:

$$\|\epsilon\|_0 = \sqrt{\frac{\int_\Omega (u-u_a)^2\,\mathrm{d}\Omega}{\int_\Omega u_a^2\,\mathrm{d}\Omega}} \quad \text{and} \quad \|\epsilon\|_1 = \sqrt{\frac{\int_\Omega (u_{,1}-u_{a,1})^2\,\mathrm{d}\Omega}{\int_\Omega u_{a,1}^2\,\mathrm{d}\Omega}} \tag{43}$$

The error in displacement and stress were compared for each of the basis function in Figs. 6–9. The convergence properties are compared with the SIHD method, a C^0-continuous displacement-based finite element solution, and a mixed finite element analysis where both the displacements and stresses are independently approximated using C^0-continuous basis functions [43,44]. A two-dimensional mixed finite element for plane-stress analysis was developed in Appendix A.

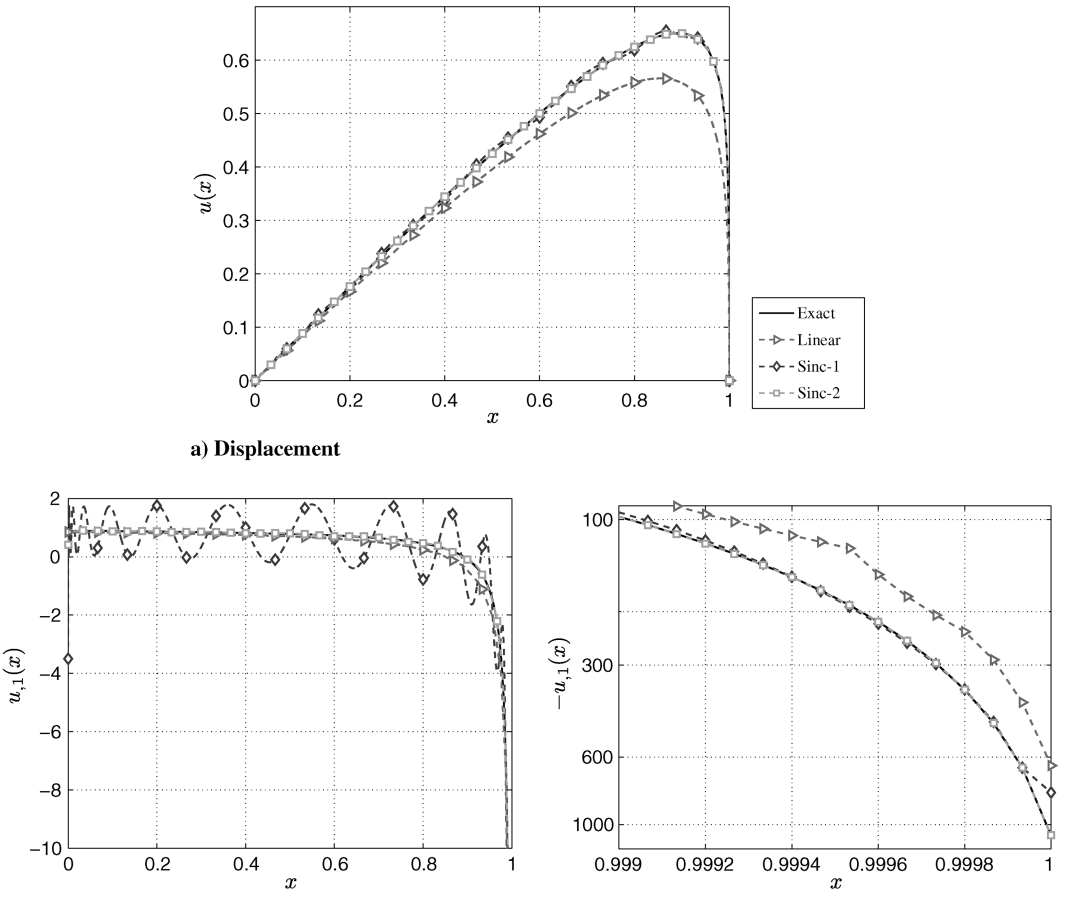

a) Displacement

b) Stress

c) Stress near the tip

Fig. 5 Displacement and stress obtained with $N = 20$ (41 sinc points) and the ILPGSM method using the Lagrange multiplier method to impose essential boundary conditions for $\delta = 0.0001$. Results are compared with analytic solution.

The finite element (FE) meshes were chosen such that the nodes were coincident to the sinc points of the SIHD and ILPGSM solutions. In implementing the SIHD method, we follow Slemp and Kapania [25]. Each analysis approach was implemented in MATLAB for the sake of comparison of computational time.

The error in displacement and stress was plotted in Fig. 6 for an axial bar having root-to-tip area ratio of 101:1 and using each of the analysis approaches. The following observations were made. The sinc-2 basis function provides a very accurate solution, with greater accuracy and a higher rate of convergence than both the C^0 finite element analysis (FEA) and the mixed FEA when the Lagrange multiplier method was used to apply the essential boundary conditions. Furthermore, the solution provides greater accuracy of the stress than the SIHD method; however, the SIHD method provides comparable accuracy for the displacements. The sinc-1 basis function using the Lagrange multiplier method to apply the essential boundary conditions resulted in accurate displacements; however, the stress was erroneously approximated. This is likely to be the result of the oscillations seen in Fig. 5. The linear basis function with the ILPGSM provides the least-accurate solution. The Lagrange multiplier method for applying the essential boundary conditions results in greater or equal accuracy to the penalty method for all basis functions.

To examine the efficiency of the ILPGSM method and compare it with the traditional and mixed FEAs, the stress accuracy was plotted against the total number of degrees of freedom and the total computational time in Fig. 7. Only ILPGSM results obtained using the sinc-2 basis function were compared with the FEAs and SIHD. The ILPGSM solution provides substantially improved accuracy over the SIHD method and traditional and mixed FEAs for equal number of degrees of freedom; however, this does not translate directly into greater efficiency. In general, the ILPGSM is less efficient than the strong form based SIHD and the FEA analyses. However, the figure indicates that the present method obtained greater accuracy of the stress for equal computational cost to the FEAs and the SIHD method if a higher accuracy is desired. The additional computational cost of the ILPGSM is the result of a large number of integration points and therefore a large number of basis function evaluations needed, and a more fully populated stiffness matrix. For $N = 150$ or a total of 305 degrees of freedom, the stiffness matrix contains 92,114 nonzero components, whereas for the C^0-continuous finite element with $N = 150$ or 301 degrees of freedom, the stiffness matrix contains only 901 nonzero components. The mixed finite element with $N = 75$ or 302 degrees of freedom, the stiffness matrix contains only 1206 nonzero components. Thus, while the present method is somewhat inefficient, the high rate of convergence may achieve improved accuracy of the stress compared with both C^0 and mixed finite element analyses for equal computational cost. Moreover, the integrated nature of SIHD and ILPGSM make them attractive candidate methods for one-step approaches for determining higher-order derivatives of displacement. These higher-order derivatives can be important such as for determining through-the-thickness interlaminar stresses in composites [25].

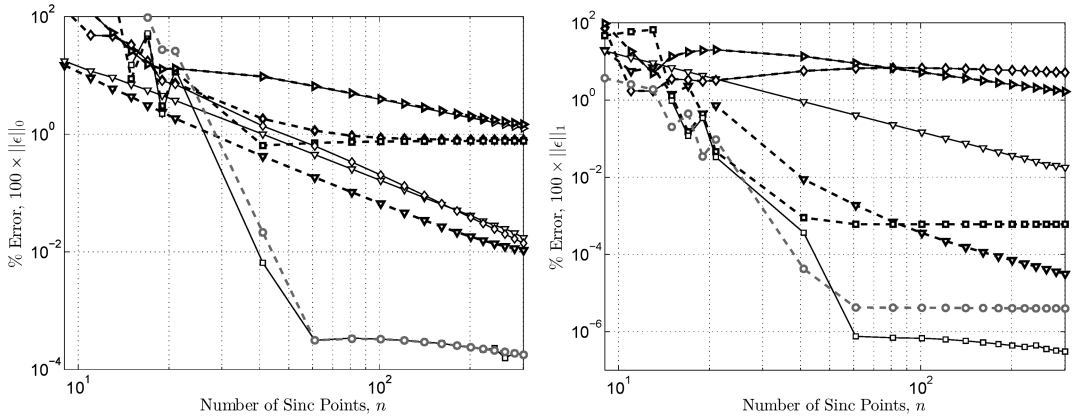

a) Error in displacement **b) Error in stress**

Fig. 6 Numerical error of the displacement and stress for tapered axial bar with taper ratio of 101:1 and increasing number of sinc points.

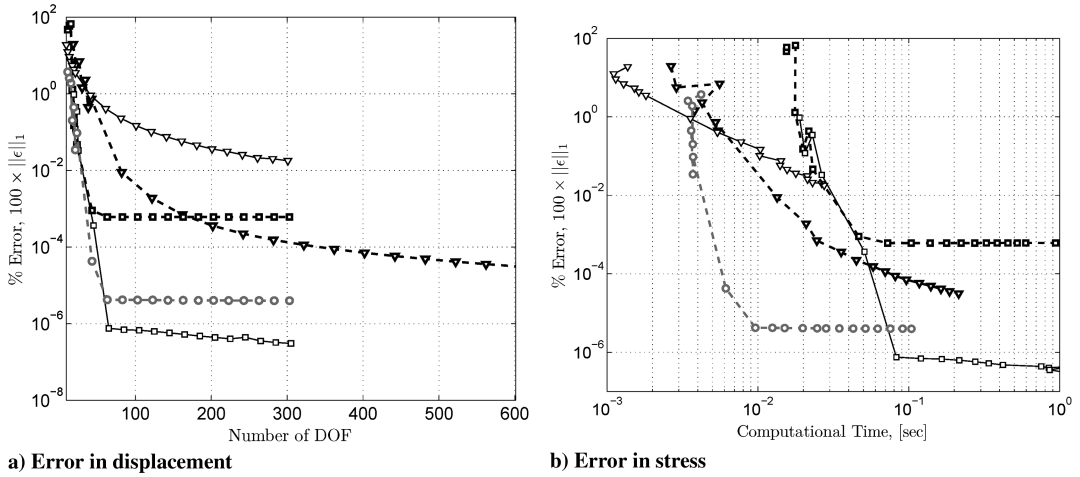

a) Error in displacement **b) Error in stress**

Fig. 7 Numerical error of the stress verses number of degrees of freedom and computational time for axial bar with taper ratio of 101:1.

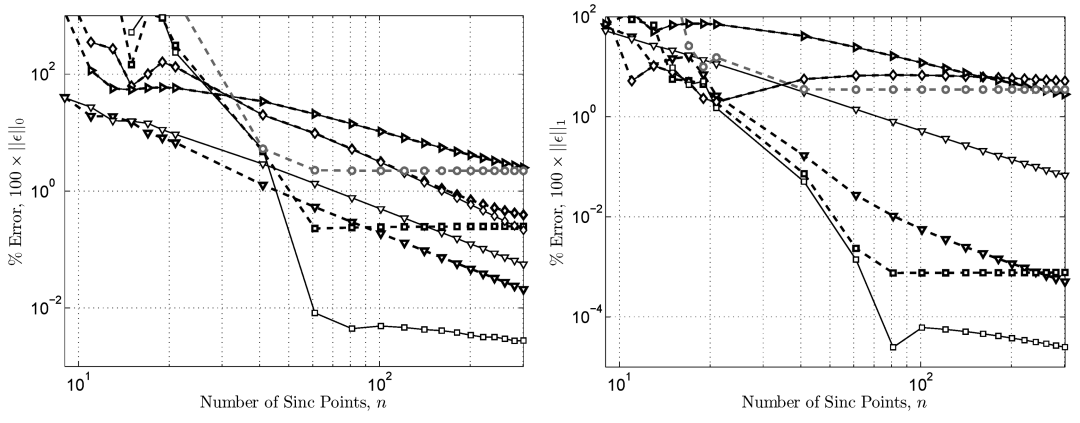

a) Error in displacement **b) Error in stress**

Fig. 8 Numerical error of the displacement and stress for tapered axial bar with taper ratio of 10, 001:1 and increasing number of sinc points.

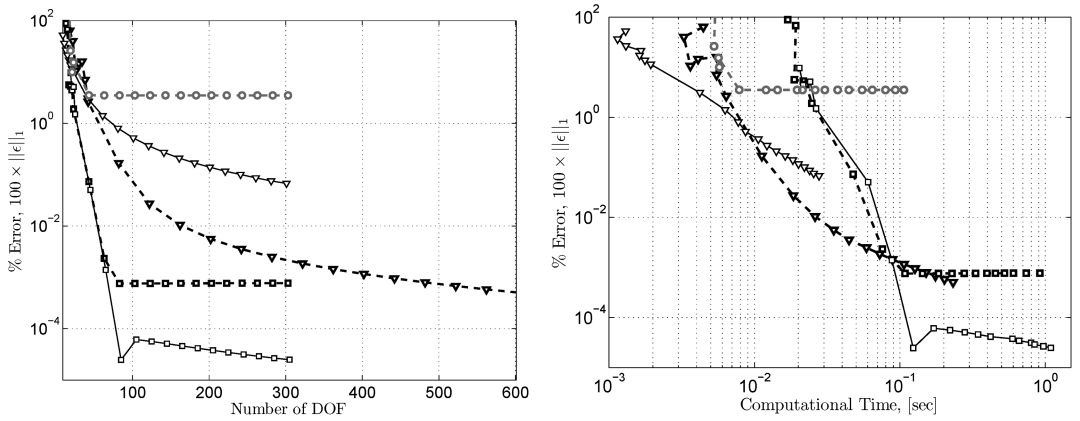

a) Error in displacement **b) Error in stress**

Fig. 9 Numerical error of the stress verses number of degrees of freedom and computational time for axial bar with taper ratio of 10, 001:1.

Similar results were obtained for an axial bar with taper ratio of 10, 001:1 in Figs. 8 and 9. Although most of the previous discussion regarding the results in Figs. 6 and 7 may also be seen in the present example, it should be noted that the ILPGSM provides far superior results to the SIHD method for the 10, 001:1 taper ratio. Furthermore, it should be noted that Fig. 9 indicates that the sinc-2 basis function and ILPGSM may be able to provide improved accuracy of stress in the presence of a stress concentration for the same computational cost as the finite element method (FEM).

V. Two-Dimensional Timoshenko Cantilever Beam

Results were also obtained by implementing the ILPGSM for a Timoshenko cantilever [45]. The formulation developed in Sec. III was used for a plane-stress analysis of a rectangular panel (see Fig. 10). The dimensions of the panel are $a = 1.0$ m long and $b = 0.2$ m wide. A parabolic shear traction is applied to the right edge ($x_1 = a$). The traction is such that

$$\sigma_{11}(a, x_2) = 0, \qquad \sigma_{12}(a, x_2) = t(x_2) = \frac{6P(bx_2 - x_2^2)}{b^3} \tag{44}$$

taking $P = 10^6$ N/m. The top ($x_2 = b$) and bottom ($x_2 = 0$) surfaces are traction-free. On the left edge, ($x_1 = 0$), the displacement is constrained such that

$$u_1(0, x_2) = \tilde{u}_1(x_2) = -\frac{2Px_2(2+\nu)}{Eb}\left(\frac{x_2}{b} - \frac{1}{2}\right)\left(\frac{x_2}{b} - 1\right)$$
$$u_2(0, x_2) = \tilde{u}_2(x_2) = \frac{6P\nu a}{Eb}\left(\frac{x_2}{b} - \frac{1}{2}\right)^2 \tag{45}$$

An analytical solution to this problem was given by Timoshenko and Goodier [45] and has been used by Batra and Zhang [29] to verify the accuracy of the SSPH meshless method. The analytical solution for displacement is

$$u_1(x_1, x_2) = -\frac{2P}{E}\left(\frac{x_2}{b} - \frac{1}{2}\right)\left[\frac{3x_1(2a - x_1)}{b^2} + \frac{x_2(2+\nu)}{b}\left(\frac{x_2}{b} - 1\right)\right]$$
$$u_2(x_1, x_2) = \frac{2P}{E}\left[\left(\frac{x_1}{b}\right)^2\left(\frac{3a}{b} - \frac{x_1}{b}\right) + 3\nu\left(\frac{a}{b} - \frac{x_1}{b}\right)\left(\frac{x_2}{b} - \frac{1}{2}\right)^2 + \frac{x_1(4+5\nu)}{4b}\right] \tag{46}$$

The ILPGSM was implemented in MATLAB R14 Service Pack 2 using all three basis functions and with the boundary conditions imposed by the penalty method and the Lagrange multiplier method. The sinc mesh size, h (see Eq. (2) and Fig. 1), was taken to be $2.0/N$. The physical domain was transformed to the computational domain by the mapping $x_1 = a(\xi - \xi_{-N})/(\xi_N - \xi_{-N})$ and $x_2 = b(\eta - \eta_{-N})/(\eta_N - \eta_{-N})$. Weight functions were chosen having the form of Eq. (39) with $\xi_{\max}$, $\xi_{\min}$, $\eta_{\max}$, and $\eta_{\min}$ chosen for each subdomain in an identical fashion to the tapered-bar problem. Displacements and

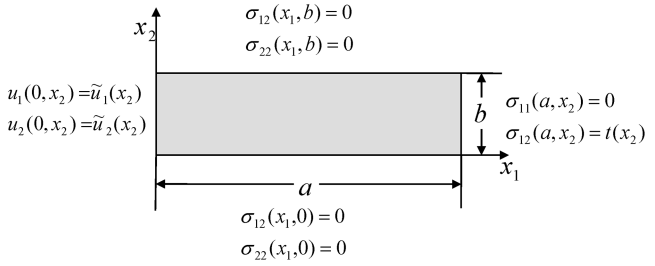

Fig. 10 Boundary conditions and dimensions of the Timoshenko cantilever problem.

stresses were obtained, using the ILPGSM with essential boundary conditions imposed using the Lagrange multiplier method and penalty method. For the sake of brevity, the contours of displacements and stresses were only presented using the sinc-2 basis function with essential boundary conditions imposed by the Lagrange multiplier method, though similar results were obtained using the other basis functions and with the penalty method for imposing essential boundary conditions. In Fig. 11, the contours of displacement and stresses were plotted from the results obtained using the sinc-2 basis function with $N = 10$ or 21 sinc points along each axis. Note that the contours are indistinguishable from the analytic solution, implying a very accurate numerical solution. Additionally, the displacement and stress contours indicated that the linear basis function performs quite well for the present problem; however, no feasible solution could be obtained using the sinc-1 basis function. It was also noted that for this case, the stresses exhibit significant oscillations similar to those seen in the tapered-bar example.

In Fig. 12, the convergence properties are compared for the ILPGSM with each basis function and both boundary conditions approaches. For the sake of comparison we implement the SIHD method, a C^0-continuous finite element with u_1 and u_2 degrees of freedom, and a mixed finite element in which u_1, u_2, σ_{11}, σ_{12}, and σ_{22} were each independently approximated using C^0 basis functions. Each approach was implemented in MATLAB for the present problem. The details for the mixed FEM solutions are provided in Appendix 1. For the FE meshes, the nodes were placed coincidental to the location of sinc points. Although we recognize that the current meshing approach may not be the most efficient approach for the present problem, it provides a reasonable mechanism for comparison. Naturally, as the number of sinc points increases, the element size decreases resulting in convergence of the FEA.

Figure 12 indicates that the sinc-2 basis function provides very accurate displacement and stress results with very few sinc points when the Lagrange multiplier method is employed; however, the solution exhibits diminishing returns beyond 21 sinc points along both axes. Nonetheless, of all the methods implemented, the sinc-2 basis function with the Lagrange multiplier approach for essential boundary conditions provides the best accuracy for displacements and stresses. The method's accuracy is a significant improvement from the SIHD method and both the C^0 and mixed finite element analysis for equal number of sinc points. If the boundary conditions are imposed by the penalty method, the sinc-2 basis function is generally less accurate than with the Lagrange multiplier method.

The linear basis function provided acceptable accuracy; however, a slow, strictly monotonic rate of convergence was achieved using the Lagrange multiplier method for imposing the essential boundary conditions. As indicated by Fig. 12, the ILPGSM with this basis function was less accurate than the SIHD method. Note that using the linear basis function resulted in comparable displacement accuracy to the standard C^0 FEM; however, the linear basis function achieved greater stress accuracy than the C^0 FEM. The mixed FEA provides

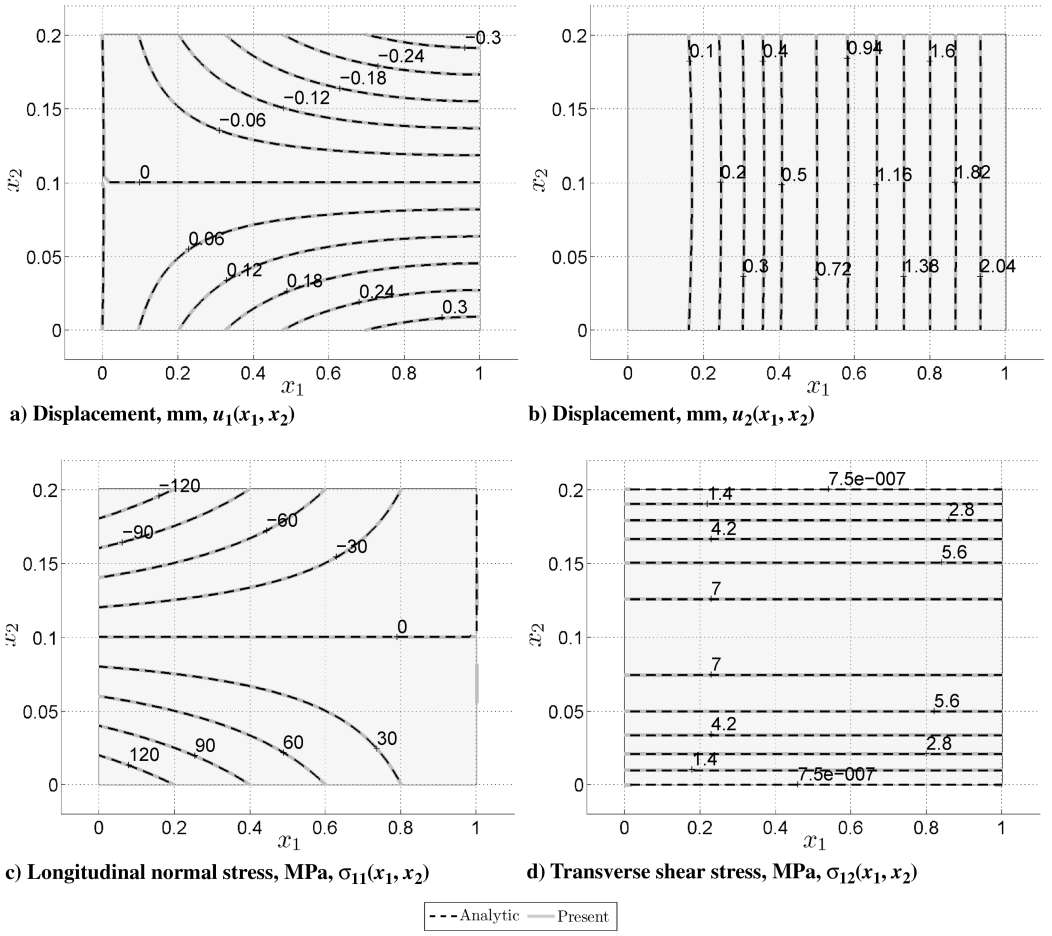

Fig. 11 Contours of displacement and stress in the Timoshenko cantilever obtained by the ILPGSM with the sinc-2 basis function ($N = 10$). The essential boundary conditions are imposed by the Lagrange multiplier method.

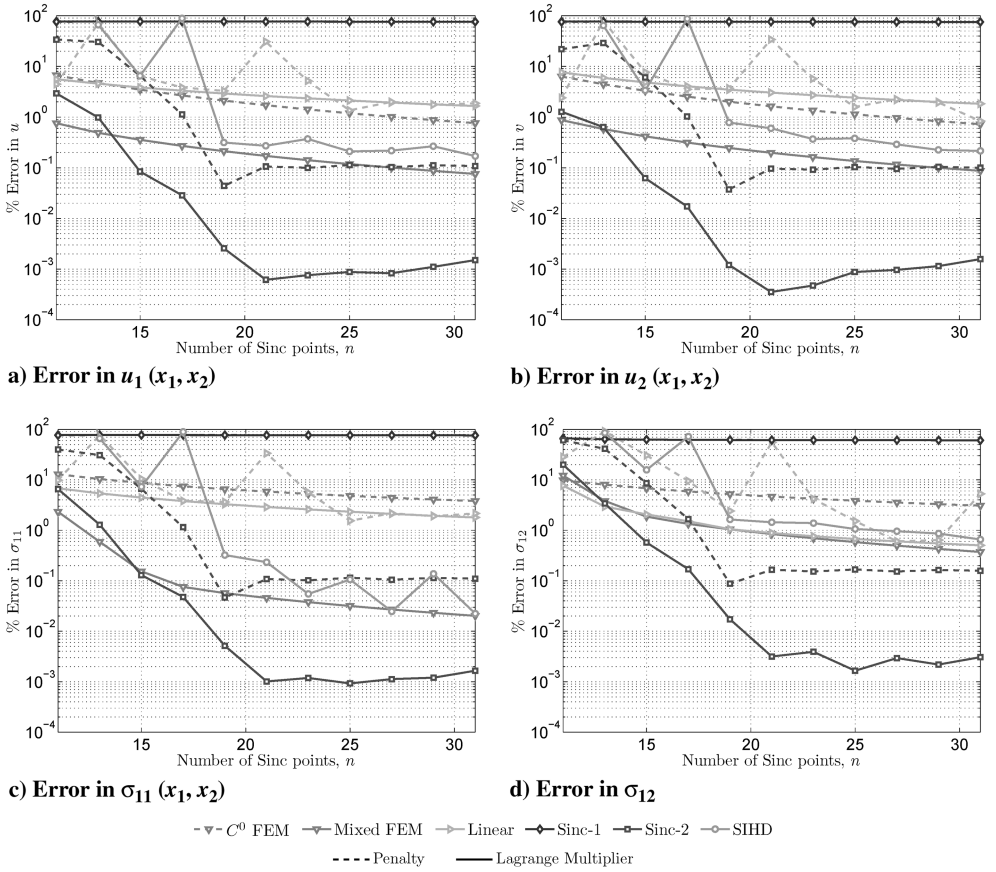

Fig. 12 Numerical error of the displacements and stresses with increasing number of sinc points. Numerical result are compared with the SIHD method, a displacement-based C^0 FEA, and a mixed FEA.

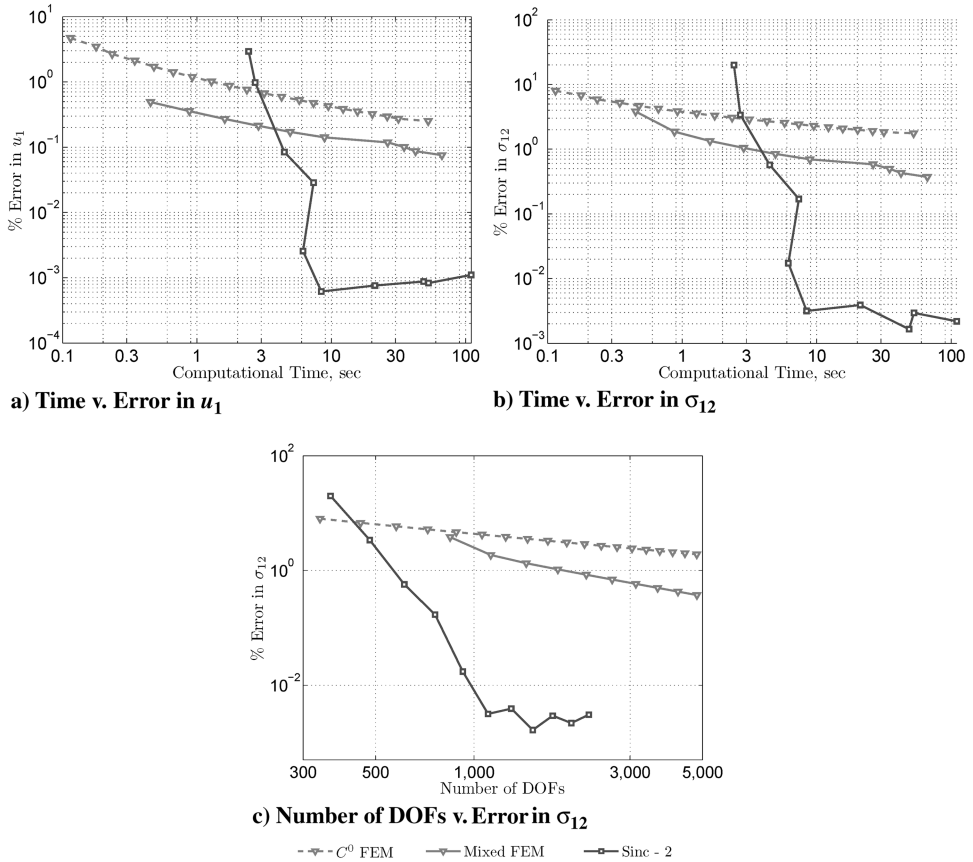

Fig. 13 Numerical error of displacement and stress versus computational time and number of degrees of freedom for solution from ILPGSM with the sinc-2 basis function and Lagrange multiplier method, a displacement-based C^0 FEA, and a mixed FEA.

greater accuracy than the linear basis function in both stresses and displacements than the linear basis function. Figure 12 also confirms that the sinc-1 basis function was not a feasible option for the analysis.

The efficiency of the sinc-2 basis function with ILPGSM and the Lagrange multiplier method was compared with the displacement and mixed FE analyses in Fig. 13. Although both the mixed and displacement-based FEAs provided acceptable accuracy (less than 1% error in the displacements) of displacements at a reduced computational cost compared with the ILPGSM, the ILPGSM can achieve greater overall accuracy. There is an initial cost penalty relative to the FEAs; however, if the analysis goal is very accurate stresses, the ILPGSM may be advantageous over traditional displacement FEA. Also, it should be noted that for the same number of degrees of freedom, the ILPGSM provides greater stress accuracy.

VI. Conclusions

A new integrated sinc method was proposed and assessed for one- and two-dimensional analysis of static structural mechanics problems. The method, named the integrated local Petrov–Galerkin sinc method (ILPGSM), is very similar to the SIHD method [15]; however, the present method uses the methodology of the meshless local Petrov–Galerkin method. Because the basis functions do not possess the Kronecker delta property, results were compared by imposing essential boundary conditions using the traditional penalty method and the Lagrange multiplier method.

We have introduced three basis functions that each use numerical indefinite integration based on the double-exponential transformation. The primary differences of the basis function are the order of the derivative initially approximated and the method of interpolating between sinc points. First-order (sinc-1) and second-order (sinc-2) basis functions using sinc interpolation and a first-order basis function using linear interpolation (linear) were introduced and assessed.

One-dimensional analysis of a fixed–fixed tapered bar whose tip area approaches zero was performed using the present method. The results indicated that the sinc-2 basis function with ILPGSM provides a highly convergent solution and performs very well in the presence of the stress concentration. The method was shown to provide greater accuracy than the SIHD method, although the cost of integration over a local subdomain is substantial. The method also suffers from a fully populated stiffness matrix, which adds additional computational time in matrix factorization when compared with the finite element method. The results indicated that despite these inefficiencies, the present method can provide additional accuracy for stresses in the presence of a stress concentration than traditional finite element methods. Because of its high rate of convergence, the ILPGSM can provide greater accuracy for equal computational cost than a displacement-based, C^0-continuous, and mixed finite element analysis.

The ILPGSM was also implemented for a two-dimensional, plane-stress elasticity problem. The results were compared with the analytic solution and the accuracy and convergence properties were compared with the SIHD method and both a displacement-based, C^0-continuous and mixed finite element analysis. For the two-dimensional problem, the sinc-2 basis function with ILPGSM once again provided greater accuracy and higher rates of convergence than the FEAs. Furthermore, the two-dimensional example also demonstrated that the ILPGSM could obtain greater accuracy of displacements and stresses for the same computational time as both a displacement-based and mixed finite element analysis.

Finally, we note that the potential benefits of the present method are assessed based on observations seen for the sample problems analyzed with the present implementation. A formal proof of improved accuracy and convergence rate is beyond the scope of this study. The comparisons made with the finite element method do not reflect an optimized implementation that may be achieved with the very mature FEM and are provided only to illustrate the potential benefits that could be achieved with additional development of the proposed method.

Appendix A: Mixed Finite Element Formulation

The mixed finite elements implemented in this paper uses Lagrange interpolation polynomials as shape functions to approximate both displacements and stress components independently. These are approximated by

$$u_1 = \mathbf{N}(\xi,\eta)\mathbf{U}_1, \quad u_2 = \mathbf{N}(\xi,\eta)\mathbf{U}_2 \quad \sigma_{11} = \bar{Q}_{11}\mathbf{N}(\xi,\eta)\mathbf{S}_{11}$$
$$\sigma_{22} = \bar{Q}_{11}\mathbf{N}(\xi,\eta)\mathbf{S}_{22}, \quad \sigma_{12} = \bar{Q}_{11}\mathbf{N}(\xi,\eta)\mathbf{S}_{12} \tag{A1}$$

where $\mathbf{N}(\xi,\eta)$ is a matrix of element shape functions that interpolate the nodal displacements and stresses, $\mathbf{U}_i$ and $\mathbf{S}_{ij}$. The plane-stress reduced stiffness, $\bar{Q}_{11}$ was used to normalize the nodal stresses. The present implementation uses four-node elements with the following shape functions:

$$\mathbf{N}(\xi,\eta) = \left\{ \frac{(\xi+1)(n+1)}{4} \quad \frac{(\xi-1)(n+1)}{-4} \quad \frac{(\xi-1)(n-1)}{4} \quad \frac{(\xi+1)(n-1)}{-4} \right\} \tag{A2}$$

where the element nodes are identified in Fig. A1.

The following functional was used to obtain the stiffness matrix:

$$\int_\Omega \sigma_{11}\delta\epsilon_{11} + \sigma_{22}\delta\epsilon_{22} + \sigma_{12}\delta\gamma_{12} + \delta\sigma_{11}(\sigma_{11} - \bar{Q}_{11}\epsilon_{11} - \bar{Q}_{12}\epsilon_{22}) + \delta\sigma_{22}(\sigma_{22} - \bar{Q}_{12}\epsilon_{11} - \bar{Q}_{22}\epsilon_{22}) + \delta\sigma_{12}(\sigma_{12} - \bar{Q}_{66}\gamma_{12})\,\mathrm{d}\Omega = \int_\Gamma t_1\delta u_1 + t_2\delta u_2\,\mathrm{d}\Gamma \tag{A3}$$

where ϵ_{ij} is expressed in terms of displacements, u_1 and u_2. If the element degree of freedom are arranged such that $\mathbf{u} = \{\mathbf{U}_1^T, \mathbf{U}_2^T, \mathbf{S}_{11}^T, \mathbf{S}_{12}^T, \mathbf{S}_{22}^T\}^T$, then the element stiffness matrix is given by

$$\mathbf{K}_{\text{ele}} = \begin{bmatrix} \mathbf{0} & \mathbf{0} & Q_{11}\mathbf{K}_{x1} & Q_{11}\mathbf{K}_{y1} & \mathbf{0} \\ \mathbf{0} & \mathbf{0} & \mathbf{0} & Q_{11}\mathbf{K}_{x1} & Q_{11}\mathbf{K}_{y1} \\ -Q_{11}K_{1x} & -Q_{12}K_{1y} & Q_{11}\mathbf{K}_{11} & \mathbf{0} & \mathbf{0} \\ -Q_{66}K_{1y} & -Q_{66}K_{1x} & \mathbf{0} & Q_{11}\mathbf{K}_{11} & \mathbf{0} \\ -Q_{12}K_{1x} & -Q_{22}K_{1y} & \mathbf{0} & \mathbf{0} & Q_{11}\mathbf{K}_{11} \end{bmatrix} \tag{A4}$$

with the following matrices definitions:

$$\mathbf{K}_{11} = \int_{-1}^{-1}\int_{-1}^{-1} N_i(\xi,\eta)N_j(\xi,\eta)|J|\,\mathrm{d}\xi\,\mathrm{d}\eta$$
$$\mathbf{K}_{x1} = \int_{-1}^{-1}\int_{-1}^{-1} N_{i,x}(\xi,\eta)N_j(\xi,\eta)|J|\,\mathrm{d}\xi\,\mathrm{d}\eta$$
$$\mathbf{K}_{y1} = \int_{-1}^{-1}\int_{-1}^{-1} N_{i,y}(\xi,\eta)N_j(\xi,\eta)|J|\,\mathrm{d}\xi\,\mathrm{d}\eta \tag{A5}$$

and with $i, j = 1, 2, \ldots 4$, $\mathbf{K}_{1x} = \mathbf{K}_{x1}^T$ and $\mathbf{K}_{1y} = \mathbf{K}_{y1}^T$. The elemental load vector is given by

$$\mathbf{F}_{\text{ele}} = \{\mathbf{F}_u, \mathbf{F}_v, \mathbf{0}, \mathbf{0}, \mathbf{0}\}^T \tag{A6}$$

where

$$\mathbf{F}_u = \int_\Gamma t_1\mathbf{N}\,\mathrm{d}\Gamma \qquad \mathbf{F}_v = \int_\Gamma t_2\mathbf{N}\,\mathrm{d}\Gamma \tag{A7}$$

For the present implementation, the elements were integrated using Gauss quadrature with two integration points on the ξ and η axis of

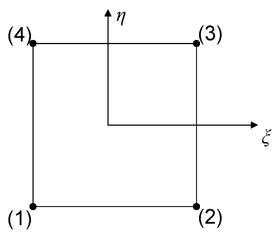

Fig. A1 Four-node finite element used in both the displacement-based C^0 and the mixed FEM with node numbering convention indicated.

the element. This integration scheme was also used for the standard C^0 finite element. The mixed and the displacement-based C^0-continuous finite element analyses for the 1-D bar problem were implemented in a similar manner; however, the integration was performed in an analytic fashion.

Acknowledgments

We would like to thank the Department of Defense and the Army Research Office for funding the National Defense Science and Engineering Graduate (NDSEG) Fellowship that supported this work. We would also like to thank the Institute for Critical Technology and Applied Science (ICTAS) at Virginia Polytechnic Institute and State University for facilities and continued support on this and other projects. We also would like to thank the reviewers for their very constructive comments and suggestions that have helped improve the quality of this paper.

References

[1] Lund, J., and Bowers, K. L., *Sinc Methods for Quadrature and Differential Equations*, Society for Industrial and Applied Mathematics, Philadelphia, 1992.

[2] Wu, X., Li, C., and Kong, W., "A Sinc-Collocation Method with Boundary Treatment for Two-Dimensional Elliptic Boundary Value Problems," *Journal of Computational and Applied Mathematics*, Vol. 196, No. 1, 2006, pp. 58–69. doi:10.1016/j.cam.2005.08.022

[3] Narasimhan, S., Majdalani, J., and Stenger, F., "A First Step in Applying the Sinc Collocation Method to the Nonlinear Navier-Stokes Equations," *Numerical Heat Transfer, Part B, Fundamentals*, Vol. 41, No. 5, 2002, pp. 447–462. doi:10.1080/104077902753725902

[4] Smith, R., Bogar, G., Bowers, K., and Lund, J., "The Sinc–Galerkin Method for Fourth-Order Differential Equations," *SIAM Journal on Numerical Analysis*, Vol. 28, No. 3, 1991, pp. 760–788. doi:10.1137/0728041

[5] El-Gamel, M., and Zayed, A., "Sinc–Galerkin Method for Solving Nonlinear Boundary-Value Problems," *Computers and Mathematics with Applications*, Vol. 48, No. 9, 2004, pp. 1285–1298. doi:10.1016/j.camwa.2004.10.021

[6] El-Gamel, M., "A Comparison Between the Sinc–Galerkin and the Modified Decomposition Methods for Solving Two-Point Boundary-Value Problems," *Journal of Computational Physics*, Vol. 223, No. 1, 2007, pp. 369–383. doi:10.1016/j.jcp.2006.09.025

[7] El-Gamel, M., "Comparison of the Solutions Obtained by Adomian's Decomposition and Wavelet-Galerkin Methods of Boundary-Value Problems," *Applied Mathematics and Computation*, Vol. 186, No. 1, 2007, pp. 652–664. doi:10.1016/j.amc.2006.08.010

[8] Al-Khaled, K., "Theory and Computation in Singular Boundary Value Problems," *Chaos, Solitons, and Fractals*, Vol. 33, No. 2, 2007, pp. 678–684. doi:10.1016/j.chaos.2006.01.047

[9] He, J.-H., "Homotopy Perturbation Technique," *Computer Methods in Applied Mechanics and Engineering*, Vol. 178, No. 3, 1999, pp. 257–262. doi:10.1016/S0045-7825(99)00018-3

[10] He, J.-H., "Homotopy Perturbation Method: A New Nonlinear Analytical Technique," *Applied Mathematics and Computation*, Vol. 135, No. 1, 2003, pp. 73–79. doi:10.1016/S0096-3003(01)00312-5

[11] El-Gamel, M., "Sinc and the Numerical Solution of Fifth-Order Boundary Value Problems," *Applied Mathematics and Computation*, Vol. 187, No. 2, 2007, pp. 1417–1433. doi:10.1016/j.amc.2006.09.049

[12] Mai-Duy, N., and Tran-Cong, T., "Approximation of Function and Its Derivatives Using Radial Basis Function Networks," *Applied Mathematical Modelling*, Vol. 27, No. 3, March 2003, pp. 197–220. doi:10.1016/S0307-904X(02)00101-4

[13] Mai-Duy, N., and Tran-Cong, T., "Numerical Solution of Differential Equations Using Multiquadratic Radial Basis Function Networks," *Neural Networks*, Vol. 14, No. 2, 2001, pp. 185–199. doi:10.1016/S0893-6080(00)00095-2

[14] Wu, X., and Ren, Y., "Differential Quadrature Method Based on the Highest Derivative and its Applications," *Journal of Computational and Applied Mathematics*, Vol. 205, No. 1, Aug. 2007, pp. 239–250. doi:10.1016/j.cam.2006.04.055

[15] Li, C., and Wu, X., "Numerical Solution of Differential Equations Using Sinc Method Based on the Interpolation of the Highest Derivatives," *Applied Mathematical Modeling*, Vol. 31, No. 1, 2007, pp. 1–9. doi:10.1016/j.apm.2006.04.013

[16] Muhammad, M., and Mori, M., "Double Exponential Formulas for Numerical Indefinite Integration," *Journal of Computational and Applied Mathematics*, Vol. 161, No. 2, 2003, pp. 431–448. doi:10.1016/j.cam.2003.05.002

[17] Mai-Duy, N., and Tanner, R., "A Spectral Collocation Method Based on Integrated Chebyshev Polynomials for Two-Dimensional Biharmonic Boundary-Value Problems," *Journal of Computational and Applied Mathematics*, Vol. 201, No. 1, April 2007, pp. 30–47. doi:10.1016/j.cam.2006.01.030

[18] Mai-Duy, N., and Tran-Cong, T., "An Integrated-RBF Technique Based on Galerkin Formulation for Elliptic Differential Equations," *Engineering Analysis with Boundary Elements*, Vol. 33, No. 2, Feb. 2009, pp. 191–199. doi:10.1016/j.enganabound.2008.05.001

[19] Bellman, R. E., and Casti, J., "Differential Quadrature and Long Term Integration," *Journal of Mathematical Analysis and Applications*, Vol. 34, No. 2, 1971, pp. 235–238. doi:10.1016/0022-247X(71)90110-7

[20] Striz, A. G., Jang, S. K., and Bert, C. W., "Nonlinear Bending Analysis of Thin Circular Plates by Differential Quadrature," *Thin-Walled Structures*, Vol. 6, No. 1, 1988, pp. 51–62. doi:10.1016/0263-8231(88)90025-0

[21] Bert, C. W., Xinwei, W., and Striz, A. G., "Differential Quadrature for Static and Free Vibration Analyses of Anisotropic Plates," *International Journal of Solids and Structures*, Vol. 30, No. 13, 1993, pp. 1737–1744. doi:10.1016/0020-7683(93)90230-5

[22] Wang, X., Bert, C. W., and Striz, A. G., "Differential Quadrature Analysis of Deflection, Buckling, and Free Vibration of Beams and Rectangular Plates," *Computers and Structures*, Vol. 48, No. 3, Aug. 1993, pp. 473–479. doi:10.1016/0045-7949(93)90324-7

[23] Kang, K., Bert, C. W., and Striz, A. G., "Vibration Analysis of Shear Deformable Circular Arches by the Differential Quadrature Method," *Journal of Sound and Vibration*, Vol. 183, No. 2, June 1995, pp. 353–360. doi:10.1006/jsvi.1995.0258

[24] Kang, K. J., Bert, C. W., and Striz, A. G., "Vibration and Buckling Analysis of Circular Arches Using DQM," *Computers and Structures*, Vol. 60, No. 1, July 1996, pp. 49–57. doi:10.1016/0045-7949(95)00375-4

[25] Slemp, W. C. H., and Kapania, R. K., "Imposing Boundary Conditions in Sinc Method Using Highest Derivative Approximation," *Journal of Computational and Applied Mathematics*, Vol. 230, No. 2, Aug. 2009, pp. 371–392. doi:10.1016/j.cam.2008.12.006

[26] Slemp, W. C. H., and Kapania, R. K., "Interlaminar Stresses by Sinc Method Based on Interpolation of the Highest Derivative," *AIAA Journal*, Vol. 46, No. 12, 2008, pp. 3128–3141. doi:10.2514/1.39613

[27] Nguyen, V. P., Rabczuk, T., Bordas, S., and Duot, M., "Meshless Methods: A Review and Computer Implementation Aspects," *Mathematics and Computers in Simulation*, Vol. 79, No. 3, Dec. 2008, pp. 763–813. doi:10.1016/j.matcom.2008.01.003

[28] Atluri, S. N., and Shen, S., "The Basis of Meshless Domain Discretization: The Meshless Local Petrov–Galerkin (MLPG) Method," *Advances in Computational Mathematics*, Vol. 23, No. 1, July 2005, pp. 73–93. doi:10.1007/s10444-004-1813-9

[29] Batra, R. C., and Zhang, G., "SSPH Basis Functions for Meshless Methods, and Comparison of Solutions with Strong and Weak Formulations," *Computational Mechanics*, Vol. 41, No. 4, 2007, pp. 527–545. doi:10.1007/s00466-007-0209-3

[30] Takahasi, H., and Mori, M., "Double Exponential Formulas for Numerical Integration," *Publications of the Research Institute for Mathematical Sciences*, Vol. 9, No. 3, 1973, pp. 721–741. doi:10.2977/prims/1195192451

[31] Muhammad, M., Nurmuhammad, A., Mori, M., and Sugihara, M., "Numerical Solution of Integral Equations by Means of the Sinc Collocation Method Based on the Double Exponential Transformation," *Journal of Computational and Applied Mathematics*,

Vol. 177, No. 2, 2005, pp. 269–286.
doi:10.1016/j.cam.2004.09.019

[32] Mori, M., "Discovery of the Double Exponential Transformation and its Developments," *Publications of the Research Institute for Mathematical Sciences*, Vol. 41, No. 4, 2005, pp. 897–935.
doi:10.2977/prims/1145474600

[33] Mori, M., and Sugihara, M., "The Double-Exponential Transformation in Numerical Analysis," *Journal of Computational and Applied Mathematics*, Vol. 127, No. 1, 2001, pp. 287–296.
doi:10.1016/S0377-0427(00)00501-X

[34] Sugihara, M., and Matsuo, T., "Recent Developments of the Sinc Numerical Methods," *Journal of Computational and Applied Mathematics*, Vols. 164–165, No. 1, 2004, pp. 673–689.
doi:10.1016/j.cam.2003.09.016

[35] Abramowitz, M., and Stegun, I. A., (eds.,) *Handbook of Mathematical Functions with Formulas, Graphs, and Mathematical Tables*, 9th printing, Dover, New York, 1972.

[36] MacLeod, A. J., "Rational Approximations, Software and Test Methods for Sine and Cosine Integrals," *Numerical Algorithms*, Vol. 12, No. 2, 1996, pp. 259–272.
doi:10.1007/BF02142806

[37] Slemp, W. C. H., Kapania, R. K., and Mulani, S. B., "Integrated Local Petrov–Galerkin Sinc Method for Structural Mechanics Problems," 50th AIAA/ASME/ASCE/AHS/ASC Structures, Structural Dynamics, and Materials Conference, AIAA Paper 2009-2392, Palm Springs, CA, May 2009.

[38] Irons, B., "Engineering Applications of Numerical Integration in Stiffness Methods," *AIAA Journal*, Vol. 4, No. 11, 1966, pp. 2035–2037.
doi:10.2514/3.3836

[39] Cook, R. D., *Concepts and Applications of Finite Element Analysis*, 2nd ed., Wiley, New York, 1981.

[40] Batra, R., and Zhang, G., "Modified Smoothed Particle Hydrodynamics (MSPH) Basis Functions for Meshless Methods, and their Application to Axisymmetric Taylor Impact Test," *Journal of Computational Physics*, Vol. 227, No. 3, Jan. 2008, pp. 1962–1981.
doi:10.1016/j.jcp.2007.10.001

[41] Sarra, S., "Integrated Multiquadric Radial Basis Function Approximation Methods," *Computers and Mathematics with Applications (1975-) / Computers & Mathematics with Applications*, Vol. 51, No. 8, April 2006, pp. 1283–1296.
doi:10.1016/j.camwa.2006.04.014

[42] Zhu, T., and Atluri, S. N., "A Modified Collocation Method and a Penalty Formulation for Enforcing the Essential Boundary Conditions in the Element Free Galerkin Method," *Computational Mechanics*, Vol. 21, No. 3, April 1998, pp. 211–222.
doi:10.1007/s004660050296

[43] Pereira, E. M. B. R., and Freitas, J. A. T., "A Hybrid-Mixed Finite Element Model Based on Legendre Polynomials for Reissner-Mindlin Plates," *Computer Methods in Applied Mechanics and Engineering*, Vol. 136, Nos. 1–2, 1996, pp. 111–126.
doi:10.1016/0045-7825(96)01061-4

[44] Pereira, E. M. B. R., and Freitas, J. A. T., "A Mixed-Hybrid Finite Element Model Based on Orthogonal Functions," *International Journal for Numerical Methods in Engineering*, Vol. 39, No. 8, 1996, pp. 1295–1312.
doi:10.1002/(SICI)1097-0207(19960430)39:8<1295::AID-NME903>3.0.CO;2-H

[45] Timoshenko, S. P., and Goodier, J. N., *Theory of Elasticity*, 3rd ed., McGraw–Hill, New York, 1970.

F. Pei
Associate Editor